L-439

ARR No. 3E25

NATIONAL ADVISORY COMMITTEE FOR AERONAUTICS

WARTIME REPORT

ORIGINALLY ISSUED
May 1943 as
Advance Restricted Report 3E25

FULL-SCALE TUNNEL INVESTIGATION OF THE PRESSURE DISTRIBUTION OVER THE TAIL OF THE P-47B AIRPLANE

By Richard C. Dingeldein

Langley Memorial Aeronautical Laboratory
Langley Field, Va.

NACA

WASHINGTON

NATIONAL ADVISORY COMMITTEE FOR AERONAUTICS

ADVANCE RESTRICTED REPORT

FULL-SCALE-TUNNEL INVESTIGATION OF THE PRESSURE DISTRIBUTION OVER THE TAIL OF THE P-47B AIRPLANE

By Richard C. Dingeldein

INTRODUCTION

At the request of the Army Air Forces, Materiel Command, measurements were made of the pressures on the tail surfaces of the Republic Aviation Corporation P-47B airplane in the NACA full-scale tunnel. The pressures were measured over the horizontal and vertical tail surfaces for several airplane angles of attack and angles of yaw and with numerous control-surface deflections to provide a check on the design loads.

This report shows the distribution of the tail normal force between the fixed and the movable surfaces, the effects of yaw and rudder deflection on the normal forces on the horizontal tail surfaces, and the similar effects of angle of attack and elevator deflection on the vertical tail surfaces. Some calculations have been made of the normal-force coefficient of the horizontal tail surface and the chordwise pressure distributions by means of existing empirical and theoretical knowledge for comparison with the experimental data. This paper was originally issued as a Memorandum Report for the Army Air Forces, Feb. 20, 1943.

SYMBOLS

c_n	section normal-force coefficient (n/qc)
C_N	normal-force coefficient (N/qS)
$dC_{N_t}/d\alpha_t$	tail effectiveness
$dC_{N_t}/d\delta_e$	elevator effectiveness

τ	ratio of the effectiveness of a change in elevator angle δ_e to the effectiveness of a change in tail angle a_t $\left(\frac{dC_{N_t}/d\delta_e}{dC_{N_t}/da_t}\right)$
p	local static pressure
q	dynamic pressure $\left(\frac{1}{2}\rho V^2\right)$
N	normal force
n	section normal force
$P_{a\delta}$	incremental additional distribution
$P_{b\delta}$	incremental basic distribution
P_δ	incremental normal-force distribution ($P_{a\delta} + P_{b\delta}$)
P_l	normal-force distribution for undeflected control surface
P	total calculated normal-force distribution ($P_l + P_\delta$)
P_x	normal-force distribution determined from pressure-distribution tests
S	area
S_t	total area of horizontal tail surface (59.6 sq ft) (includes area blanketed by fuselage)
S_s	stabilizer area (37.6 sq ft)
S_e	elevator area, including balance (22 sq ft)
S_f	fin area (13.6 sq ft)
S_r	rudder area, including balance (12.9 sq ft)
u	local velocity in boundary layer
V	velocity
c	chord (length behind hinge line on movable surface)
a_t	angle of attack of horizontal tail surface

α_T angle of attack of thrust axis relative to free-stream direction, degrees

ψ angle of yaw, degrees; positive when left wing moves forward

δ control-surface deflection, degrees; positive with elevator down or rudder left

ϵ downwash angle at tail measured relative to free-stream direction, degrees

i_t angle of stabilizer setting with respect to the thrust axis, degrees; positive with trailing edge down

ρ mass density of air, slugs per cubic foot

Subscripts:

o free stream

s stabilizer

e elevator

f fin

r rudder

t horizontal tail surface

is isolated tail

APPARATUS AND TESTS

The Republic P-47B is a high-altitude pursuit airplane (figs. 1 and 2) weighing about 13,500 pounds and equipped with a Pratt & Whitney R-2800-21 engine and a four-blade Curtiss electric propeller. The tail surfaces have approximately elliptical chord distribution although they are not of elliptical plan form. The elevator and rudder are provided with inset hinge balances averaging 16.4 and 14.8 percent of the average control-surface chord, respectively. The elevator and the rudder on the airplane tested are

fabric-covered and are fitted with control tabs. The ratio of the average tab chord to the average control-surface chord is about 0.46 for the elevator and 0.35 for the rudder. The stabilizer incidence for the tests was $1\frac{1}{2}^{\circ}$ and the leading edge of the fin was offset 1° left from the longitudinal axis of the airplane.

A total of 437 flush-type orifices was installed in the empennage as follows: 140 in the stabilizer, 150 in the elevator, 68 in the fin, and 79 in the rudder. The orifice locations and rib dimensions are given in figures 3 and 4 and in tables I, II, and III.

All tests were made with the propeller removed. At zero angle of yaw and at airplane angles of attack of 0° and 15.6°, the tail-surface pressures were measured for several angular deflections of the elevator. (See table IV.) Similar tests were made for a range of rudder deflections at yaw angles from 0° to 9°. One test at an intermediate angle of attack of 5.1° and several tests at an angle of attack just above the stall (17.1°) were also made.

The elevator was deflected 3° for the rudder tests. The elevator and rudder tabs were locked at settings of -2° and 0°, respectively. The thrust axis, the stabilizer chord, and the longitudinal axis of the airplane were used as reference lines from which angle of attack, elevator deflection, and rudder deflection were measured.

The tunnel airspeed for the tests at the two low angles of attack was 87 miles per hour. The tests at the two high angles of attack were made at an airspeed of 63 miles per hour.

RESULTS AND DISCUSSION

Isometric charts of typical pressure distributions over the P-47B tail surfaces at three angles of attack for different control-surface settings and yaw angles are shown in figures 5 to 15. No unusual tail load distributions are indicated by these results. For high angles of attack of the fixed surfaces the expected peak loads occur on the leading edge of the fixed surface, and for large deflections of the movable surfaces the expected peak loads occur near the hinge line. A peak load occurs on the elevator mass balance for elevator angles in which the nose of the balance projects appreciably beyond the stabilizer surface. (See fig. 6.)

A reduction in normal force on the ribs adjacent to the fuselage is clearly shown by the data. This reduction in normal force, which increases with angle of attack, results from the wake of the fuselage and wing-fuselage juncture. (See figs. 5 to 8.) A large reduction in the pressure peaks at the right side of the horizontal tail surface was measured at $\alpha_T = 17.1^\circ$ (fig. 7). The decrease is due to local stalling which occurred on this side of the horizontal tail when the wing stalled.

The pressure distribution on the vertical tail surface with the rudder deflected -9° at an angle of attack of 0° and an angle of yaw of 0° is shown in figure 9. Similar data at an angle of yaw of 9° for rudder deflections of 0° and -6° are shown in figures 10 and 11, and the data for an angle of attack of 15.6° are shown in figures 12 to 14. Results at the stalled angle of attack of 17.1° with the airplane yawed 9° are presented in figure 15.

Normal-Force Coefficients

The average normal-force coefficients that were found by integrating the span load distribution curves are given in table IV. All of the coefficients used in this report are given in terms of free-stream dynamic pressure except where noted. Because the pressure distribution between ribs 5 and 6 was not measured, the following method was used for estimating the load on the fuselage: The spanwise curve of normal-force distribution was faired as a straight line between ribs 5 and 6 as an upper limit of the possible load. For the lower limit, the load curve was faired to zero at the juncture of the stabilizer and fuselage. The stabilizer normal-force coefficients C_{N_S} were then plotted (fig. 16) for each of the two fairings over a range of elevator deflections at angles of attack of 0° and 15.6° and compared with similar values determined from unpublished force tests made in the NACA full-scale tunnel. From this comparison, it was found that about two-thirds of the difference between the normal forces given by the two fairings should be applied as the load on the fuselage. The stabilizer span loadings were accordingly faired for each of the tests.

Curves of the span load distribution for representative test conditions are shown for the stabilizer in figure 17 and for the elevator in figure 18. Combined distributions for the horizontal tail showing the variation of the load with

elevator deflection and the effect of yaw on the horizontal tail are given in figure 19. Typical span loadings on the fin and rudder are shown in figure 20 and the loading over the entire vertical tail surface for each of these conditions is shown in figure 21.

The variations of the normal-force coefficients on the fixed and movable surfaces with airplane angle of attack are shown in figure 22 for an elevator setting of 3°. The normal-force coefficients of the stabilizer and the elevator are the same at an angle of attack of 4°. At $\alpha_T = 15.6°$ the stabilizer normal-force coefficient is about three times as great as the elevator normal-force coefficient.

The normal force on the fin increases with angle of attack for the zero-yaw condition due to an apparent increase in sidewash across the fin from left to right. The load on the rudder remains negligibly small over the entire range of angle of attack.

The effects of elevator deflection on the stabilizer and elevator normal-force coefficients for $\alpha_T = 0°$ and $\alpha_T = 15.6°$ are shown in figure 23.

The variation of C_N with angle of yaw for the vertical tail surface at airplane angles of attack of 0° and 15.6° is shown in figures 24 and 25, respectively. Similar curves of C_N plotted against rudder deflection for different yaw angles are given in figures 26 and 27. The increase of the normal force on the fin with yaw is 50 percent less at an angle of attack of 15.6° than at an angle of attack of 0°.

The effects of rudder deflection and yaw angle on the normal force on the horizontal tail are shown in figures 28 and 29, respectively, and similar effects of elevator deflection on the vertical-tail loadings are shown in figure 30. The effects are small but measurable.

Prediction of Forces on Horizontal Tail Surface

An attempt has been made to determine whether agreement exists between the measured pressure distribution on the P-47B horizontal tail surface and the distribution predicted by existing empirical and theoretical knowledge. Owing to the lack of sufficient data relative to the sidewash angles at the tail, a similar correlation for the vertical tail has not

been made. The steps followed in predicting the pressure distributions on the horizontal tail surface of the P-47B airplane are:

(1) Calculation of the isolated-tail characteristics from the tail dimensions

(2) Determination of the resultant downwash and dynamic-pressure distribution at the tail plane

(3) Determination of the average normal-force coefficient of the horizontal tail surface for any angle of attack and elevator deflection

(4) Calculation of the chord load distribution corresponding to the calculated section normal-force coefficients

Isolated-tail characteristics. - The normal-force coefficient of an isolated tail can be expressed in the form

$$(C_{N_t})_{is} = \left(\frac{dC_{N_t}}{d\alpha_t}\right)_{is} (\alpha_t + \tau\delta_e)$$

where

$$\tau = \left(\frac{dC_{N_t}/d\delta_e}{dC_{N_t}/d\alpha_t}\right)_{is}$$

For the isolated horizontal tail surface of the P-47B airplane, the tail effectiveness $(dC_{N_t}/d\alpha_t)_{is}$, which depends mainly on the aspect ratio, was found to be 0.062 from reference 1. The corresponding value of τ, which depends mainly on the ratio of the elevator area to the total tail area, was found to be 0.54 (reference 1). The elevator effectiveness $(dC_{N_t}/d\delta_e)_{is}$ is therefore 0.033.

Some error may exist in these empirical values inasmuch as the slope $(dC_{N_t}/d\alpha_t)_{is}$ also depends on the various other features of the tail design, such as the chord distribution, the elevator cut-out, and the gap between the stabilizer and the elevator. The chord distribution appears to have little effect, provided the tail has rounded tips. Measurements made to investigate the effect of cut-out on $(dC_{N_t}/d\alpha_t)_{is}$ showed this effect to be almost negligible (reference 1).

A gap between the stabilizer and the elevator is, in general, detrimental although the published data on the subject appear to be incomplete.

Downwash at tail. - The effective angle of attack of the horizontal tail surface α_t may be expressed as follows:

$$\alpha_t = \alpha_T - \epsilon + i_t$$

The downwash at the tail ϵ may be considered as the resultant downwash of the wing, the fuselage, and the wing-fuselage juncture. The wing downwash can be computed with considerable accuracy by the methods of reference 2; however, the effect of the fuselage and wing-fuselage juncture on the resultant downwash at the tail is not readily calculable and may be the source of considerable inaccuracy for airplanes with a poor wing-fuselage juncture. The effective angles of attack of the P-47B tail were calculated to be 0.9° and 8.3° at airplane angles of attack of 0° and 15.6°. The values given for α_t are corrected for jet-boundary effects at the tail (reference 3).

Dynamic-pressure distribution across horizontal tail. - In the presence of the airplane, the normal force on the tail is reduced owing to the loss of dynamic pressure at the tail due to the wing and fuselage wakes. A few calculations, based on the methods of reference 2, showed that the horizontal tail surface was above the wing wake for angles of attack below 15.6° and was at the top of the wing wake at $\alpha_T = 15.6°$. The change in dynamic pressure at the tail due to the fuselage boundary layer has been calculated by the methods of references 4 and 5. Figure 31 shows the loss in dynamic pressure at the tail due to the wing and to the fuselage wakes at $\alpha_T = 15.6°$ and the resultant dynamic-pressure variation across the tail semispan.

Figure 32 shows the variation of the product of local dynamic-pressure ratio and local chord along the tail semispan for $\alpha_T = 15.6°$. In accordance with the experimental results of figure 19 the value of $(q/q_0)c$ shown in figure 32 at the fuselage center line has been taken as 40 percent of the peak value of $(q/q_0)c$. The resulting dynamic-pressure distributions resemble the actual span-loading curves. Weighted average values of q/q_0 across the tail span were calculated to be 0.90 at $\alpha_T = 0°$ and 0.78 at $\alpha_T = 15.6°$.

Normal-force coefficient of horizontal tail. - The average normal-force coefficient at the tail for any particular

angle of attack and elevator deflection is determined from the isolated-tail characteristics and from calculated values of ϵ and q/q_o. A summary of typical calculations of normal-force coefficients on the P-47B tail together with values obtained from the pressure measurements follows:

α_T	C_L	δ_e	α_t	$\frac{q}{q_o}$	τ (Calculated)	$\left(\frac{dC_{N_t}}{d\alpha_t}\right)_{is}$ (Calculated)	$\left(\frac{dC_{N_t}}{d\delta_e}\right)_{is}$		$\left(C_{N_t}\right)_{is}$	
							Calculated	Experimental	Calculated	Experimental
0	0.103	0	0.9	0.90	0.54	0.062	0.033	0.032	0.056	-0.042
15.6	1.236	0	8.3	.78	.54	.062	.033	.029	.515	.517
15.6	1.253	5	8.3	.78	.54	.062	.033	.029	.680	.671

Some discrepancy exists at $\alpha_T = 0^\circ$ between the experimental and the calculated values of C_{N_t}. Inasmuch as the experimental value of C_{N_t} is negative for an apparent positive tail angle of attack, it appears likely that the fuselage, the effects of which were neglected in the calculation, may have considerable influence on the resultant downwash at the tail at this angle of attack. Figures 33 and 34 show the stabilizer span load distribution measured at $\alpha_T = 0^\circ$ for elevator deflections of 0° and 3°, respectively. It is seen that the down load is greatest at the inboard sections of the stabilizer; this fact indicates an apparent increase in downwash at these sections due to the fuselage. The effect of the fuselage on the resultant downwash at the tail at $\alpha_T = 15.6^\circ$ appears to be negligible.

The normal-force coefficient at any section may be determined from the calculated values of $(C_{N_t})_{is}$ because, for a surface having an elliptical chord distribution, the normal-force coefficient at any section will be constant along the tail span and equal to $(C_{N_t})_{is}$. A comparison is given in figure 35 of the section normal-force coefficients calculated by the afore-mentioned methods and the values determined from the pressure measurements. The agreement between the calculated and the experimental results is good. It should be noted (fig. 35) that the forces normal to the surface will be greatest at the outboard sections of the horizontal tail inasmuch as the dynamic pressures at these sections are greatest. This distribution of normal force may result in greater values of bending moments than those that would be calculated for the structural design of the tail based on conventional methods.

Chord load distribution. - The chordwise pressure distribution corresponding to any section normal-force coefficient may be calculated by following the methods given in references 6 and 7. Based on the section normal-force coefficients as determined herein, calculations of the chordwise pressure distribution for one representative chord have been made and are compared with the experimental results in figures 36 to 39. The calculations were made for an NACA 0006 section, which is very similar to the airfoil section used in the P-47B tail. The pressure-distribution curves have been calculated for a flap chord equal to the elevator chord plus balance (figs. 36 and 37) and for a flap chord equal to the elevator chord (figs. 38 and 39). The comparison between the calculated and the measured results indicates that best agreement would have been obtained if the flap chord were measured from a point midway between the nose of the elevator and the elevator hinge line.

SUMMARY OF RESULTS

The pressure-distribution measurements over the P-47B tail surfaces show the following results:

1. There was a smaller loading at the inboard sections of the horizontal tail surface and a greater loading at the outboard sections of the horizontal tail surface than would be expected for a surface having an elliptical chord distribution. The reduction in section normal force at the ribs adjacent to the fuselage was due to the fuselage boundary layer and increased with angle of attack.

2. The normal-force coefficient of the fin at zero yaw angle increased from -0.066 at an angle of attack of 0° to 0.016 at an angle of attack of 15.6°, but the load on the rudder was negligibly small for all angles of attack.

3. The increase of normal force on the fin with yaw was about 50 percent less at an angle of attack of 15.6° than at 0°.

4. The effect of elevator deflection on the vertical-tail effectiveness and the effect of rudder deflection on the horizontal-tail effectiveness were small but measurable.

5. The pressure distribution over the horizontal tail of the P-47B airplane was approximated by existing theoretical and empirical methods.

Langley Memorial Aeronautical Laboratory,
National Advisory Committee for Aeronautics,
Langley Field, Va.

REFERENCES

1. Silverstein, Abe, and Katzoff, S.: Aerodynamic Characteristics of Horizontal Tail Surfaces. Rep. No. 688, NACA, 1940.

2. Silverstein, Abe, and Katzoff, S.: Design Charts for Predicting Downwash Angles and Wake Characteristics behind Plain and Flapped Wings. Rep. No. 648, NACA, 1939.

3. Silverstein, Abe, and Katzoff, S.: Experimental Investigation of Wind-Tunnel Interference on the Downwash behind an Airfoil. Rep. No. 609, NACA, 1937.

4. Silverstein, Abe: Toward a Rational Method of Tail-Plane Design. Jour. Aero. Sci., vol. 6, no. 9, July 1939, pp. 361-369.

5. Goett, Harry J., and Pass, H. R.: Effect of Propeller Operation on the Pitching Moments of Single-Engine Monoplanes. NACA A.C.R., May 1941.

6. Jacobs, Eastman N., and Rhode, R. V.: Airfoil Section Characteristics as Applied to the Prediction of Air Forces and Their Distribution on Wings. Rep. No. 631, NACA, 1938.

7. Allen, H. Julian: Calculation of the Chordwise Load Distribution over Airfoil Sections with Plain, Split, or Serially Hinged Trailing-Edge Flaps. Rep. No. 634, NACA, 1938.

TABLE I

CHORDWISE LOCATIONS OF HORIZONTAL-TAIL ORIFICES

[Stations in in. from leading edge]

Stabilizer

Rib	Tube	Station
1, 10	1	9
	2	13 3/8
2, 9	0	0
	1, 9	1
	2, 10	2
	3, 11	4
	4, 12	6
	5, 13	10
	6, 14	14
	7, 15	18
	8, 16	21
3, 8	0	0
	1, 9	1
	2, 10	2
	3, 11	4
	4, 12	6 1/2
	5, 13	11
	6, 14	16 1/8
	7, 15	21
	8, 16	27
4, 7	0	0
	1, 9	1 1/2
	2, 10	3
	3, 11	5 7/8
	4, 12	9 7/8
	5, 13	15 15/16
	6, 14	21 15/16
	7, 15	28
	8, 16	33 3/4
5, 6	0	0
	1, 9	1 7/8
	2, 10	3 7/8
	3, 11	7 7/8
	4, 12	11 13/16
	5, 13	19 7/8
	6, 14	28
	7, 15	34
	8, 16	39

Elevator

Rib	Tube	Station
1, 10	3	0
	4, 11	1/2
	5, 12	2
	6, 13	3 3/4
	7, 14	6 3/8
	8, 15	9 7/8
	9, 16	12 1/4
	10, 17	14 7/8
2, 9	17	0
	18, 25	7/8
	19, 26	1 3/4
	20, 27	3 5/8
	21, 28	6 9/16
	22, 29	9 5/8
	23, 30	12 1/2
	24, 31	16 1/8
3, 8	17	0
	18, 25	3/4
	19, 26	1 1/2
	20, 27	3 1/2
	21, 28	6 7/8
	22, 29	10 13/16
	23, 30	15 1/4
	24, 31	18 3/4
4, 7	17	0
	18, 25	3/4
	19, 26	2
	20, 27	4 1/2
	21, 28	8 1/16
	22, 29	12 3/16
	23, 30	16 1/16
	24, 31	20 1/8
5, 6	17	0
	18, 25	9/16
	19, 26	1 7/8
	20, 27	4 3/16
	21, 28	6 7/8
	22, 29	9 15/16
	23, 30	13
	24, 31	15 7/8

TABLE II

CHORDWISE LOCATIONS OF VERTICAL-TAIL ORIFICES

[Stations in in. from leading edge]

Fin

Rib	Tube	Station
11	1, 3	$11\frac{5}{8}$
	2, 4	$14\frac{1}{4}$
12	0	0
	1, 8	$1\frac{1}{2}$
	2, 9	3
	3, 10	5
	4, 11	9
	5, 12	13
	6, 13	18
	7, 14	$21\frac{3}{4}$
13	0	0
	1, 8	1
	2, 9	$2\frac{1}{2}$
	3, 10	5
	4, 11	9
	5, 12	15
	6, 13	$21\frac{1}{2}$
	7, 14	$27\frac{1}{2}$
14	0	0
	1, 9	$1\frac{1}{2}$
	2, 10	3
	3, 11	5
	4, 12	8
	5, 13	14
	6, 14	22
	7, 15	28
	8, 16	33
15	0	0
	1, 9	2
	2, 10	4
	3, 11	6
	4, 12	11
	5, 13	$19\frac{1}{2}$
	6, 14	$29\frac{1}{2}$
	7, 15	$39\frac{1}{2}$
	8, 16	$45\frac{1}{2}$

Rudder

Rib	Tube	Station
11	5	0
	6, 10	$1\frac{5}{16}$
	7, 11	$3\frac{7}{8}$
	8, 12	$9\frac{3}{4}$
	9, 13	$13\frac{1}{4}$
12	15	0
	16, 22	$\frac{9}{16}$
	17, 23	$1\frac{11}{16}$
	18, 24	$3\frac{1}{2}$
	19, 25	$8\frac{1}{4}$
	20, 26	$10\frac{5}{8}$
	21, 27	$12\frac{3}{8}$
13	15	0
	16, 23	$\frac{1}{2}$
	17, 24	$1\frac{3}{4}$
	18, 25	$4\frac{1}{8}$
	19, 26	$8\frac{1}{16}$
	20, 27	$11\frac{1}{4}$
	21, 28	$13\frac{3}{4}$
	22, 29	$16\frac{7}{8}$
14	17	0
	18, 25	$\frac{1}{2}$
	19, 26	$1\frac{3}{4}$
	20, 27	4
	21, 28	$7\frac{7}{16}$
	22, 29	12
	23, 30	$15\frac{11}{16}$
	24, 31	$19\frac{7}{8}$
15	17	0
	18, 25	$\frac{5}{16}$
	19, 26	$1\frac{1}{2}$
	20, 27	$3\frac{5}{8}$
	21, 28	8
	22, 29	$13\frac{3}{16}$
	23, 30	$18\frac{11}{16}$
	24, 31	$23\frac{7}{16}$
16	0	0
	6	$1\frac{3}{8}$
	1, 7	$3\frac{13}{16}$
	2, 8	$6\frac{9}{16}$
	3, 9	$11\frac{9}{16}$
	4, 10	$18\frac{7}{16}$
	5, 11	$24\frac{5}{16}$

TABLE III

CHORDS AT ORIFICE STATIONS

[Measured in in.]

Rib	Total chord	Fixed surface	Movable surface (1)	Balance
1, 10	$30\frac{1}{2}$	$14\frac{1}{2}$	$9\frac{3}{4}$	$6\frac{1}{4}$
2, 9	40	22	$14\frac{3}{8}$	$3\frac{5}{8}$
3, 8	$49\frac{3}{4}$	$28\frac{3}{4}$	$17\frac{1}{2}$	$3\frac{1}{2}$
4, 7	$57\frac{1}{2}$	$35\frac{1}{2}$	$18\frac{5}{8}$	$3\frac{3}{8}$
5, 6	58	40	$14\frac{3}{4}$	$3\frac{1}{4}$
11	$31\frac{1}{2}$	16	$8\frac{3}{4}$	$6\frac{3}{4}$
12	$39\frac{1}{4}$	$23\frac{1}{4}$	11	5
13	$49\frac{1}{4}$	$29\frac{1}{2}$	$14\frac{3}{4}$	5
14	$58\frac{3}{4}$	$35\frac{3}{4}$	18	5
15	74	$47\frac{1}{2}$	$21\frac{1}{2}$	5
16	26	---	21	5

[1]Dimensions given are from hinge line to trailing edge.

TABLE IV

NORMAL-FORCE COEFFICIENTS FOR ALL TEST CONDITIONS

[Based on free-stream dynamic pressure]

Run	α (deg)	ψ (deg)	δ_e (deg)	δ_r (deg)	C_{N_s}	C_{N_e}	C_{N_f}	C_{N_r}
1	0	0	0	0	-0.057	-0.007	-0.043	0.023
2	0	0	3	0	.001	.136	-.066	.008
3	0	0	10	0	.176	.374	-.091	.018
4	0	0	-5	0	-.168	-.187	-.071	-.002
5	0	0	3	3	------	.129	.000	.093
6	0	0	3	-3	------	.115	-.109	-.053
7	0	0	3	-6	------	.116	-.156	-.137
8	0	0	3	-9	.017	.111	-.222	-.204
9	0	3	3	0	.010	.125	.136	.028
10	0	3	3	-3	.022	.137	.092	-.032
11	0	6	3	0	.031	.126	.284	.069
12	0	6	3	-3	.028	.124	.202	-.035
13	0	6	3	-6	.010	.123	.180	-.109
14	0	9	3	0	.003	.117	.469	.059
15	0	9	3	-6	.030	.116	.374	-.072
16	0	9	3	-9	.015	.118	.274	-.166
17	5.1	0	3	0	.204	.178	-.020	.010
18	15.6	0	0	0	.564	.130	.002	.027
19	15.6	0	5	0	.675	.264	.043	.024
20	15.6	0	-5	0	.474	.004	.035	.022
21	15.6	0	-15	0	.289	-.290	.032	.026
22	15.6	0	-20	0	.193	-.416	-.010	.022
23	15.6	0	3	0	.649	.229	.016	.009
24	15.6	0	3	-3	.629	.226	-.039	-.047
25	15.6	0	3	-6	.655	.223	-.073	-.103
26	15.6	0	3	-9	.671	.232	-.140	-.200
27	15.6	0	3	-12	.654	.180	-.189	-.268
28	15.6	0	3	-15	.631	.225	-.201	-.310
29	15.6	3	3	0	.641	.225	.107	.036
30	15.6	3	3	-3	.729	.217	.057	-.047
31	15.6	3	3	-6	.634	.227	.007	-.121
32	15.6	6	3	0	.653	.229	.211	.054
33	15.6	6	3	-3	.641	.226	.146	-.016
34	15.6	6	3	-6	.639	.222	.099	-.114
35	15.6	9	3	0	.670	.219	.314	.085
36	15.6	9	3	-6	.661	.236	.204	-.071
37	15.6	9	3	-9	.664	.229	.122	-.180
38	17.1	0	3	0	.784	.249	.008	.047
39	17.1	9	3	0	.776	.294	.299	.057
40	17.1	9	3	-6	.745	.266	.222	-.053
41	17.1	9	3	-9	.750	.263	.167	-.158

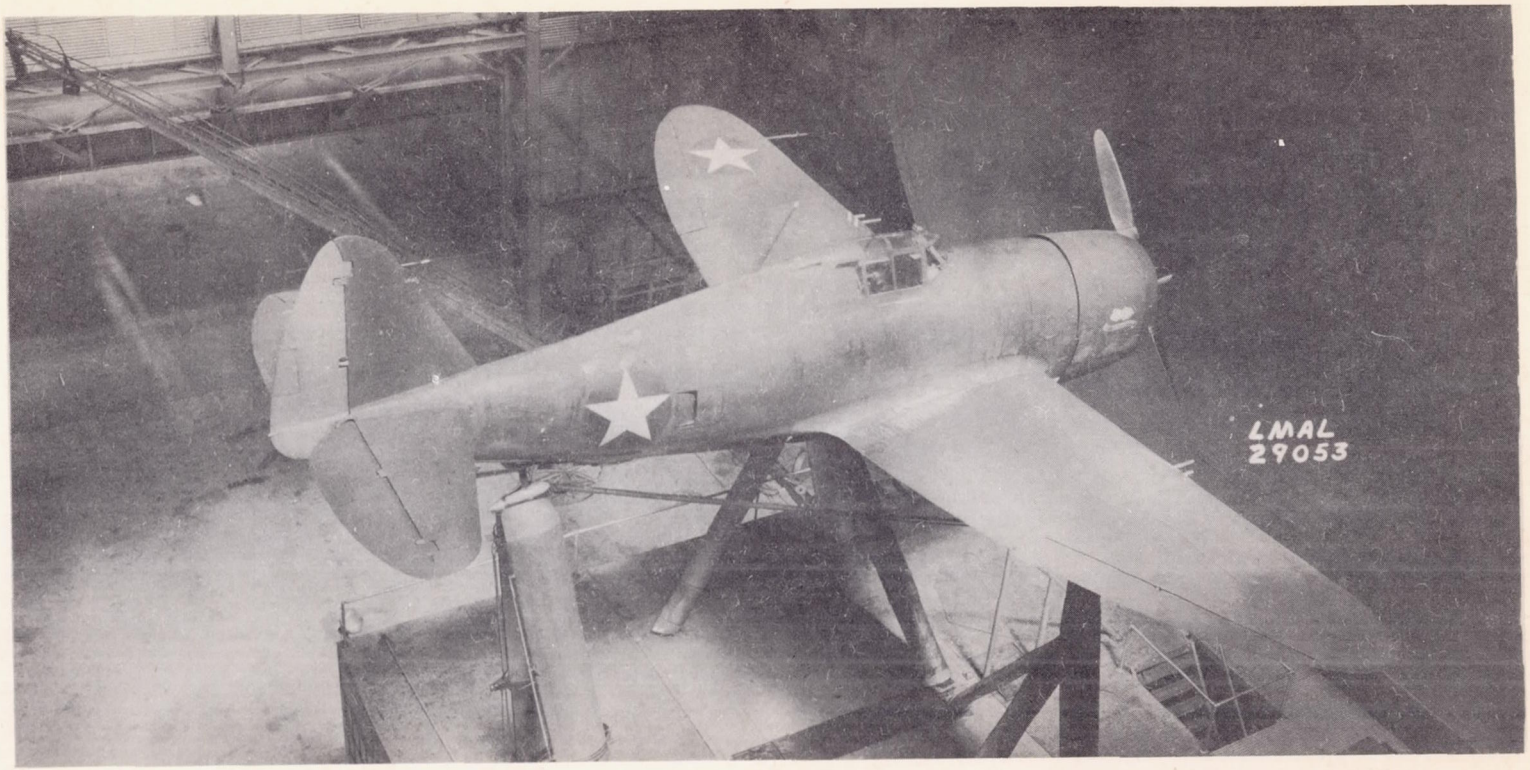

Figure 1.- The P-47B airplane mounted in the full-scale tunnel.

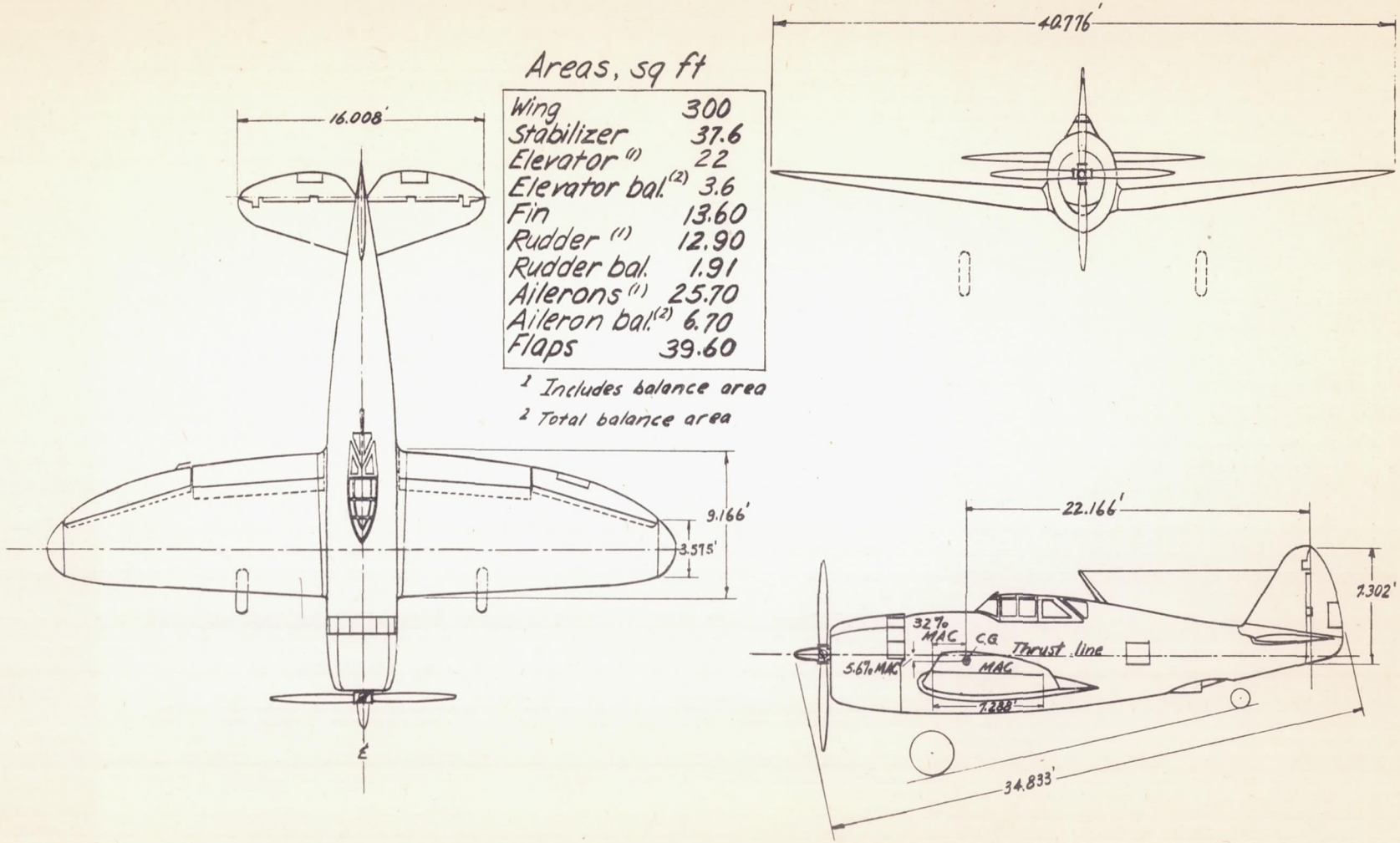

Figure 2.- Three-view drawing of the P-47B airplane.

NACA

Figs. 3,15

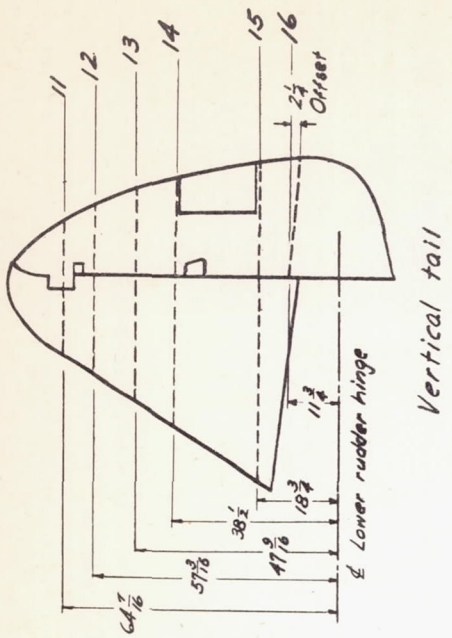

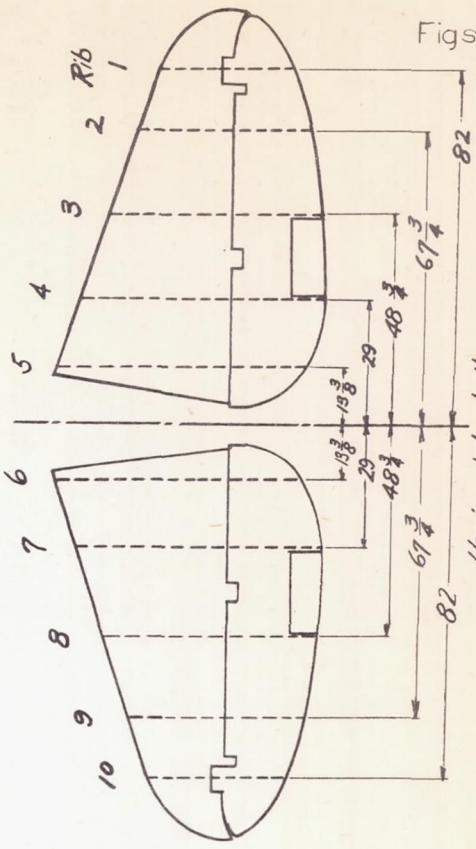

Figure 3.- Location of orifice stations (in.).

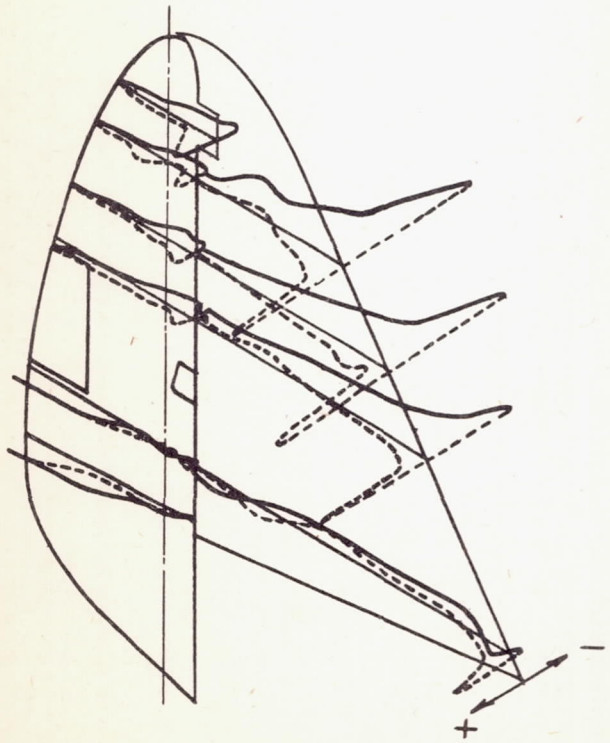

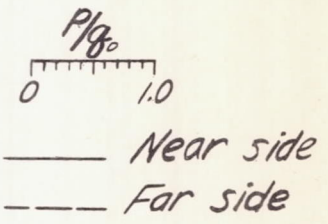

$\alpha_T = 17.1°$; $\psi = 9°$;
$\delta e = 3°$; $\delta r = 0°$.

Figure 15.- Vertical tail surface pressure distribution.

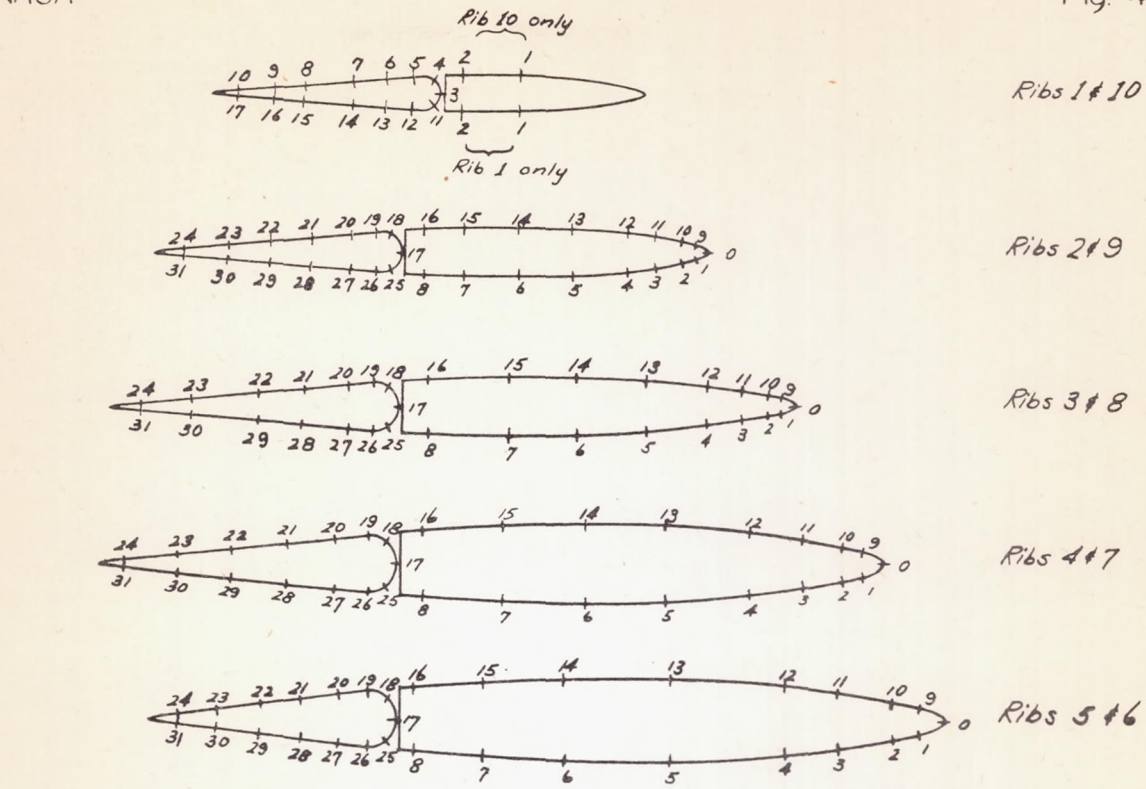

Figure 4(a).- Chordwise locations of horizontal-tail orifices.

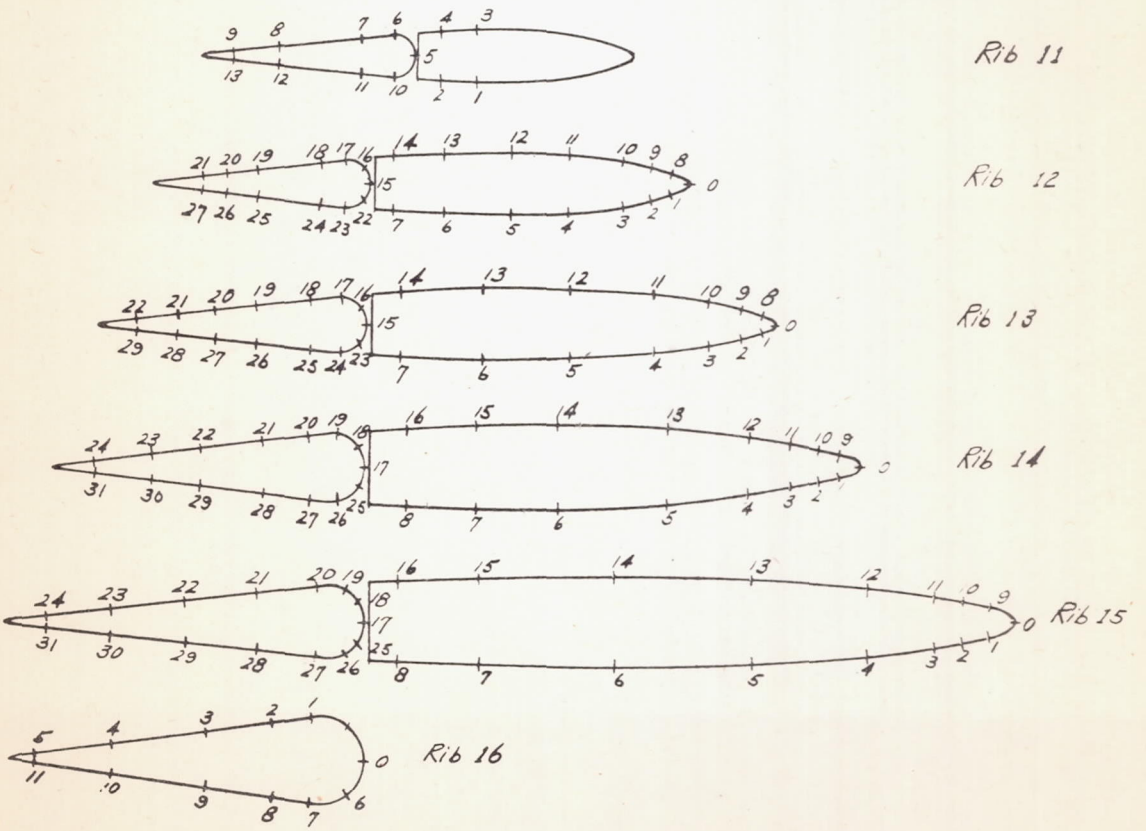

Figure 4(b) - Chordwise locations of vertical-tail orifices.

NACA

Figs. 5,6

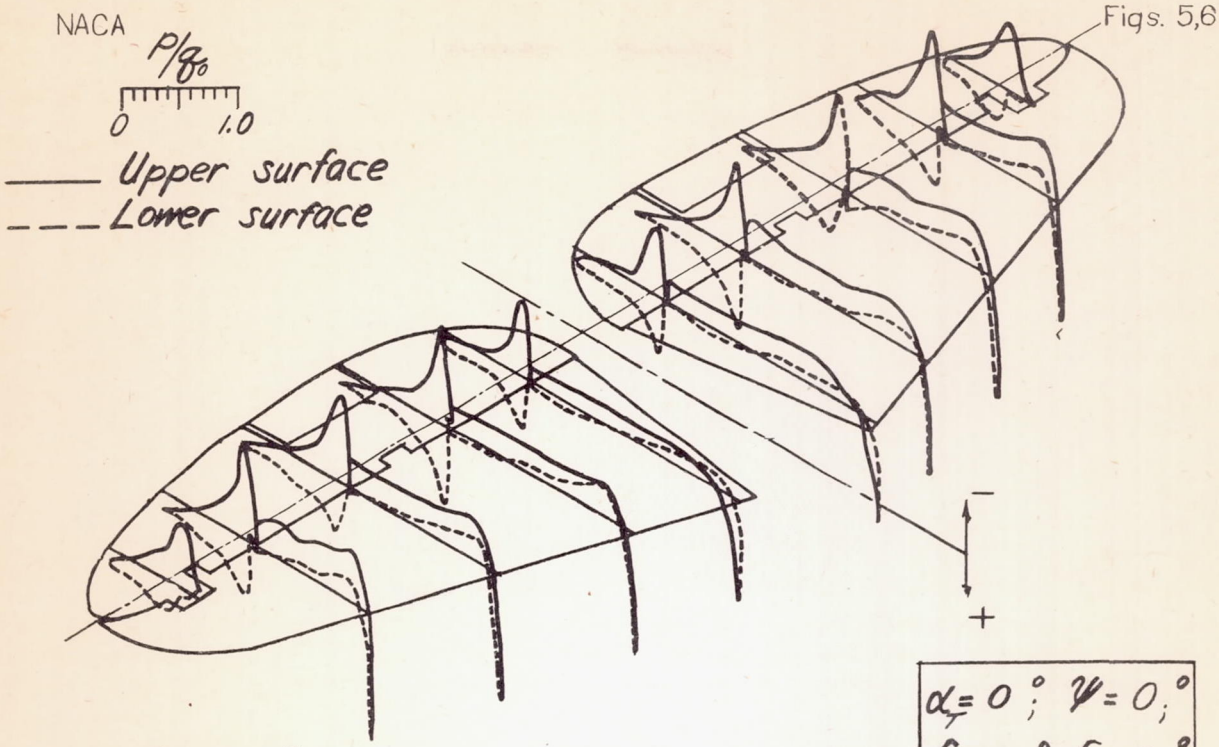

Figure 5. - Horizontal tail surface pressure distribution.

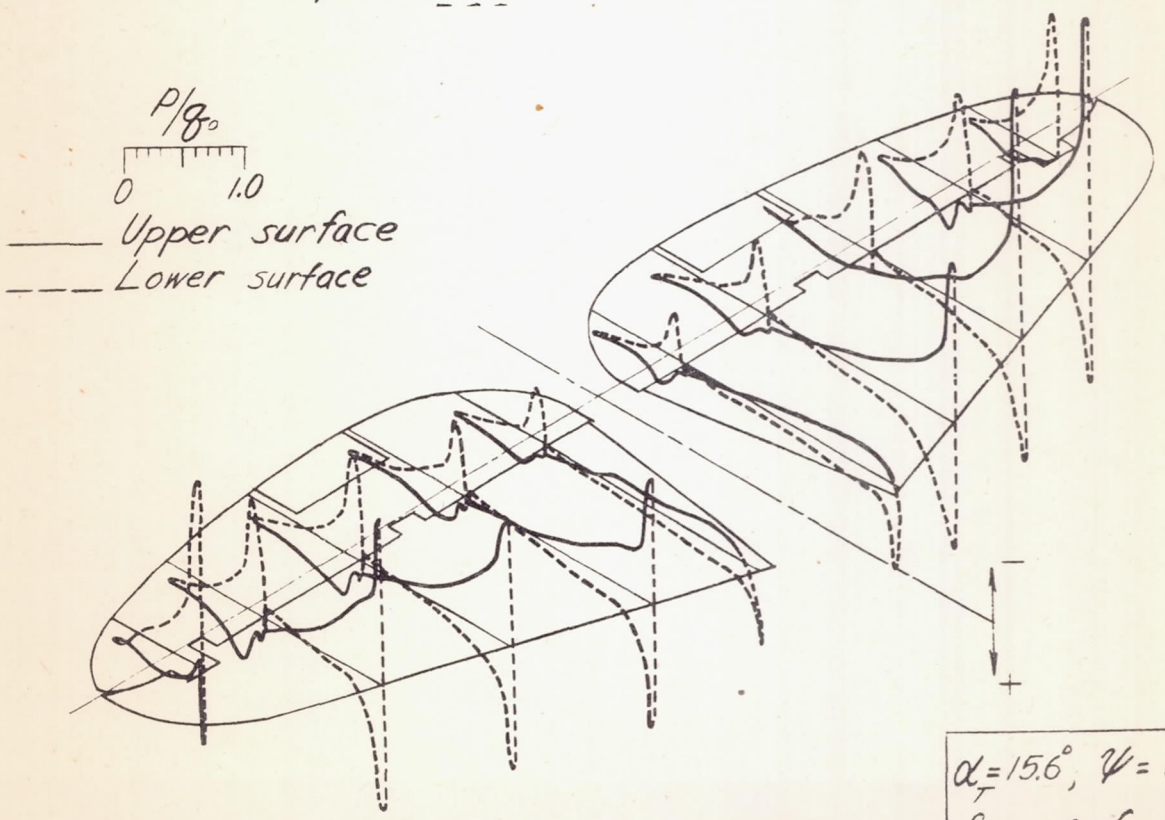

Figure 6. - Horizontal tail surface pressure distribution.

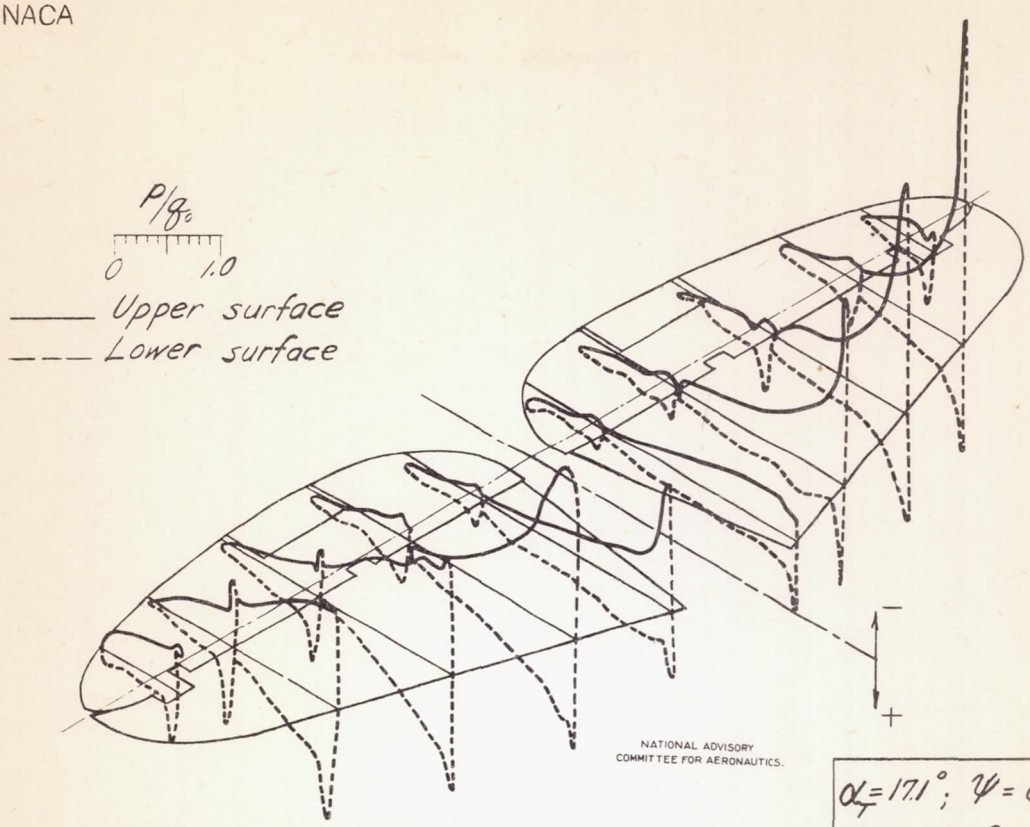

Figure 7. -Horizontal tail surface pressure distribution.

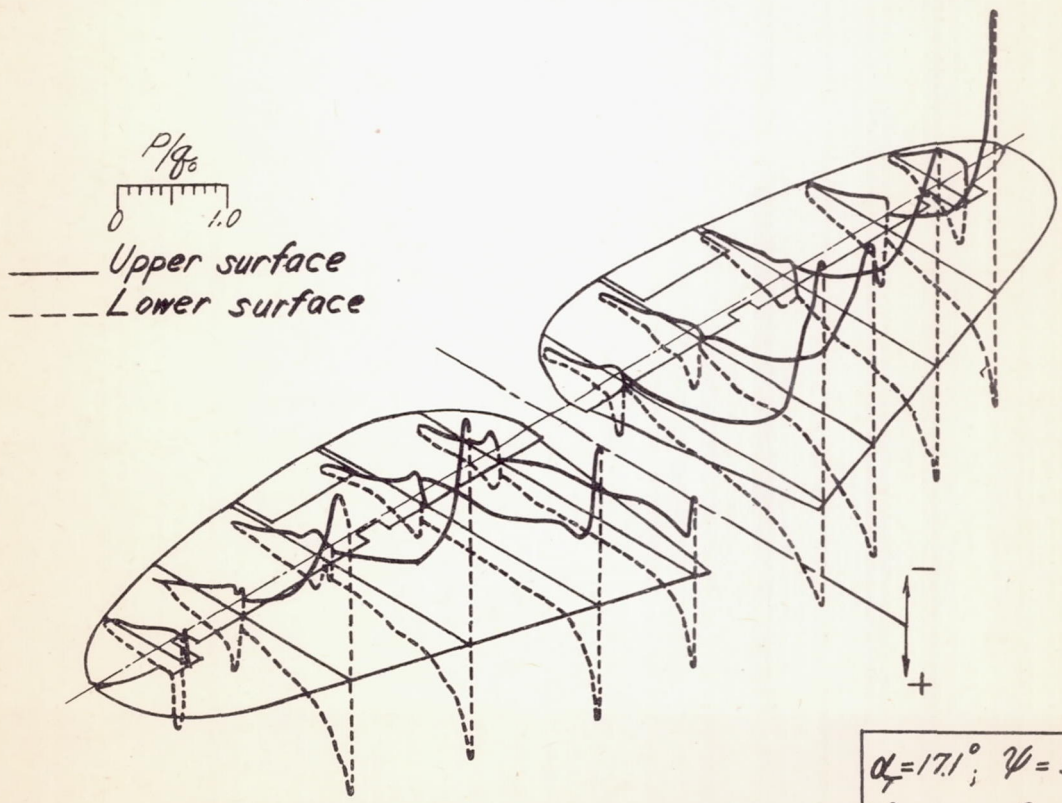

Figure 8. -Horizontal tail surface pressure distribution.

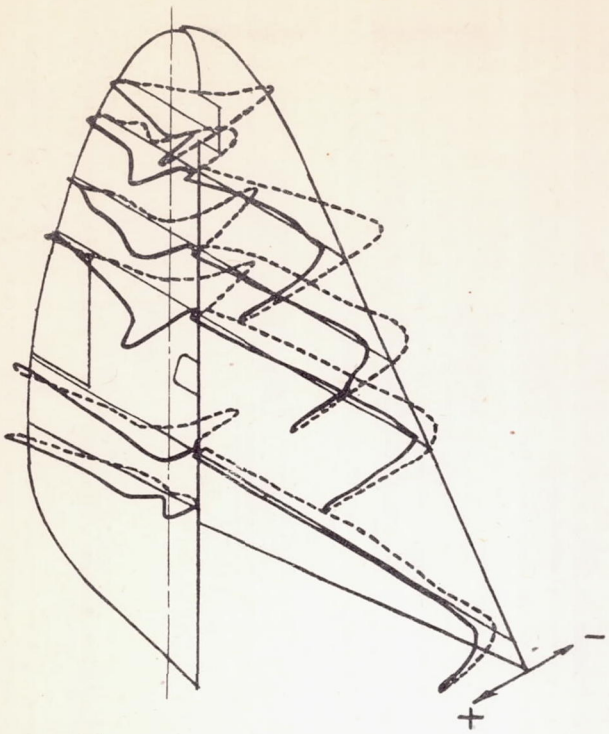

Figure 9. - Vertical tail surface pressure distribution

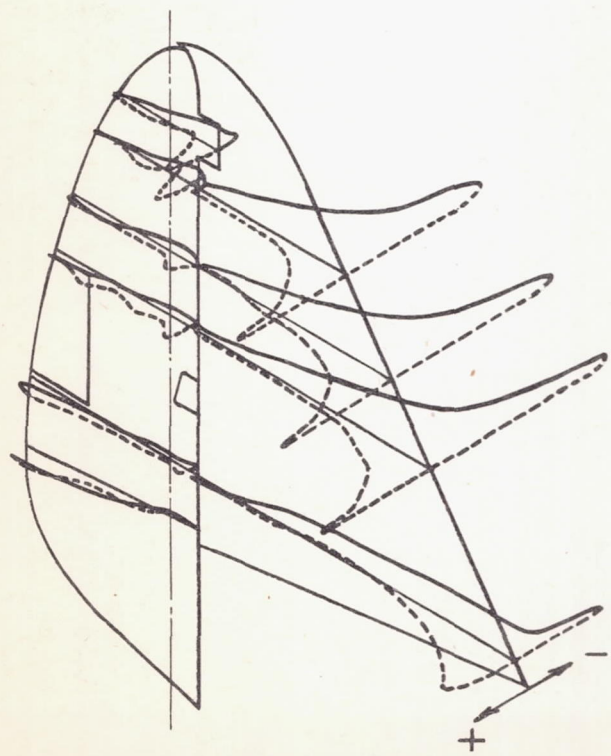

Figure 10. - Vertical tail surface pressure distribution.

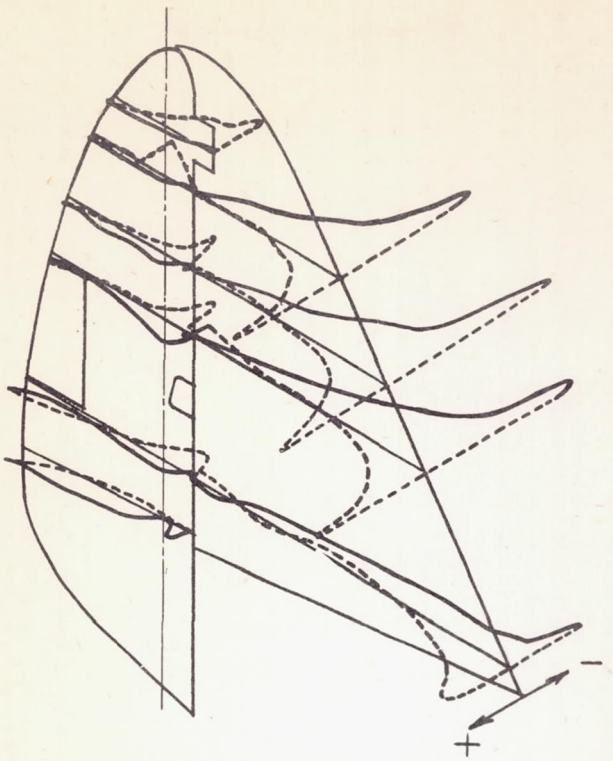

Figure 11. - Vertical tail surface pressure distribution.

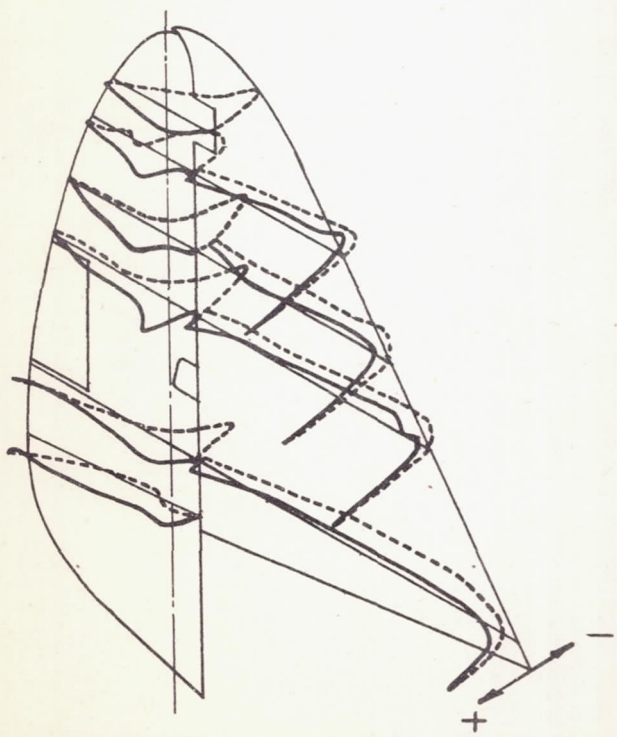

Figure 12. - Vertical tail surface pressure distribution.

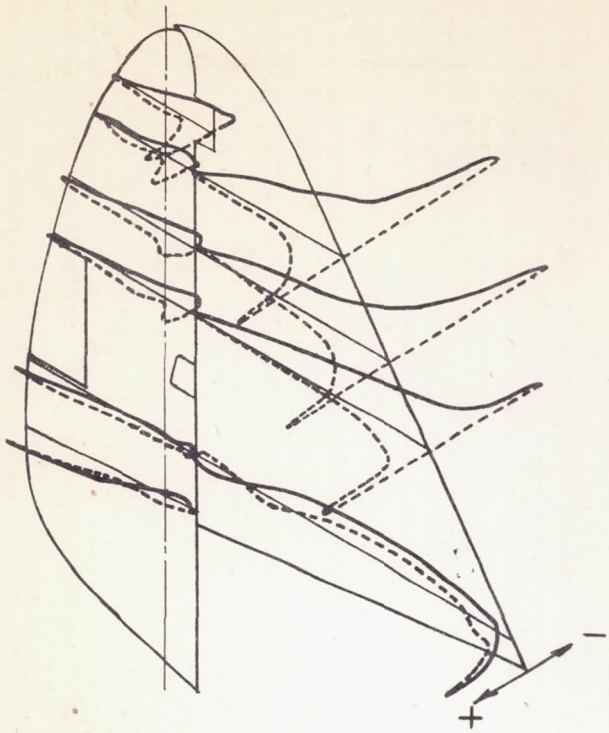

Figure 13. - Vertical tail surface pressure distribution

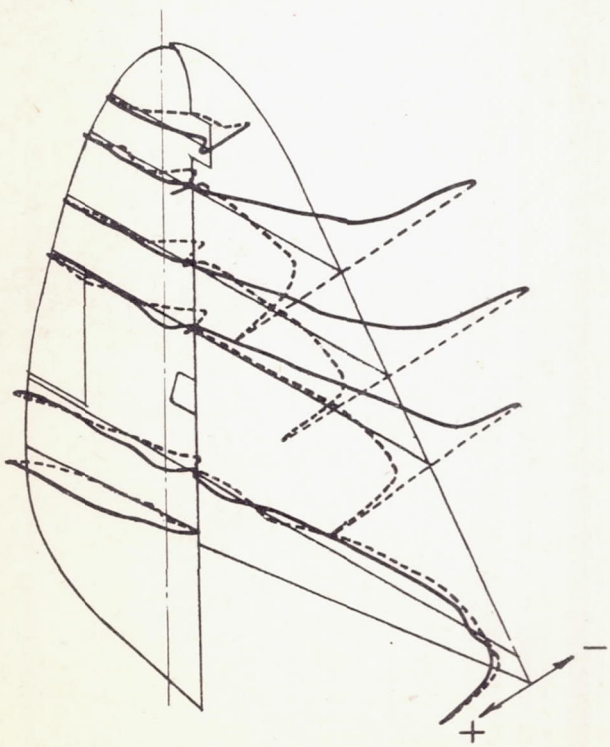

Figure 14. - Vertical tail surface pressure distribution.

NATIONAL ADVISORY
COMMITTEE FOR AERONAUTICS.

L-439

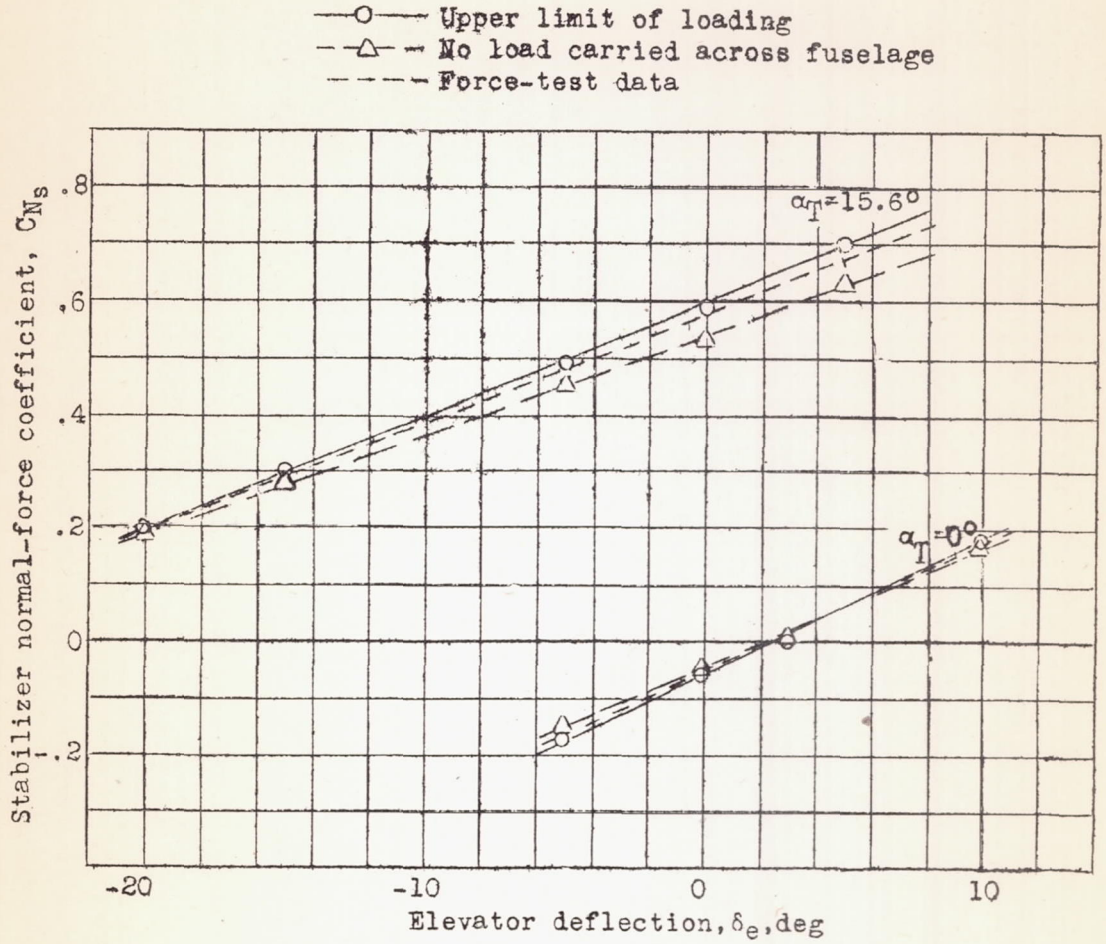

Figure 16.- Determination of stabilizer loading carried across fuselage.

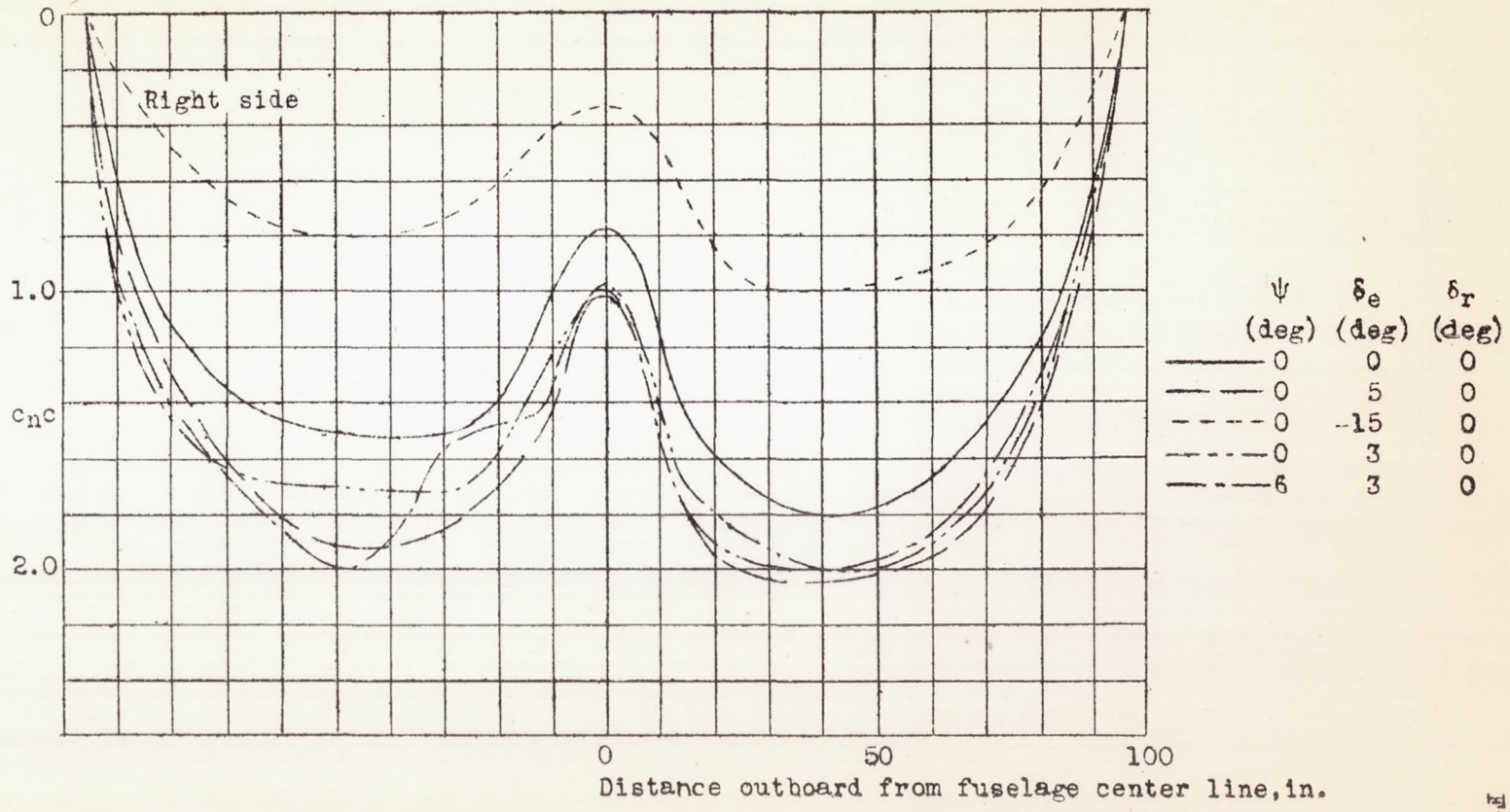

Figure 17.- Stabilizer span loadings, α_T 15.6°.

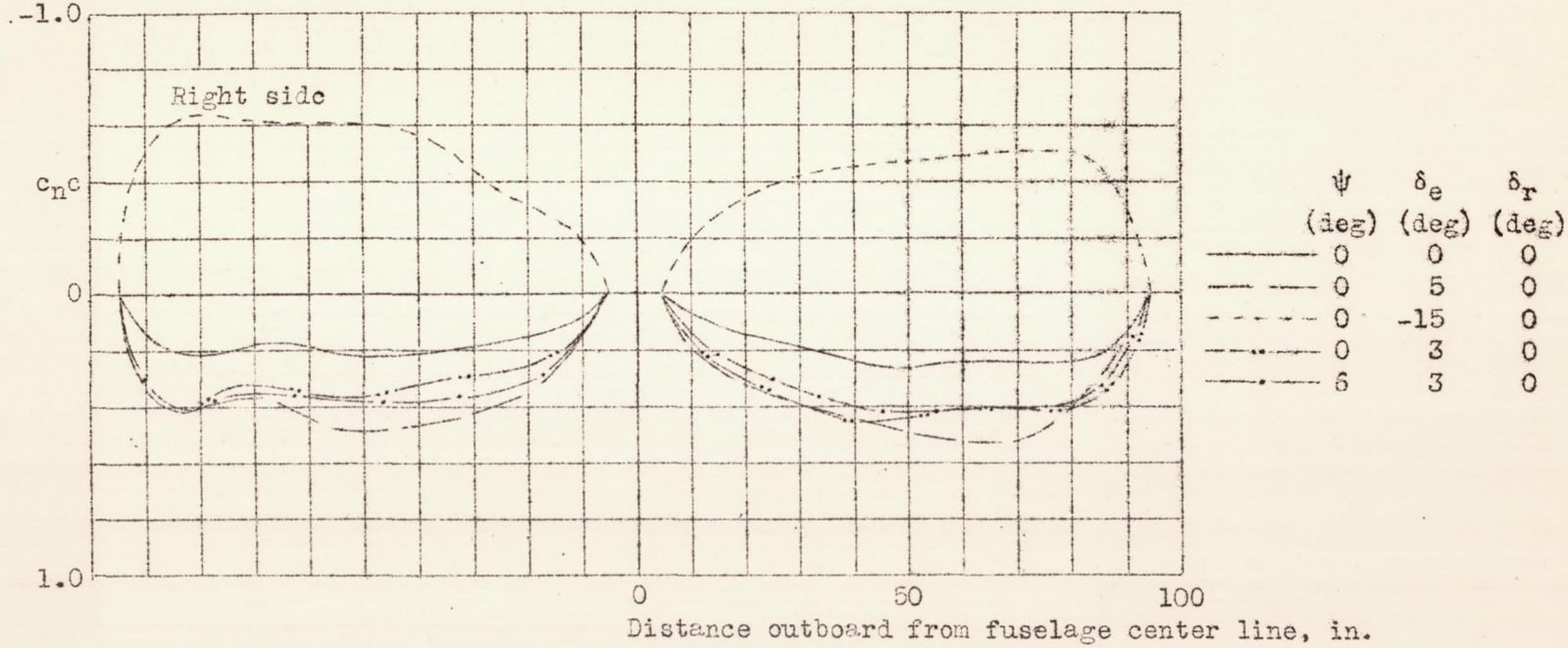

Figure 18.- Elevator span loadings, α_T, 15.6°.

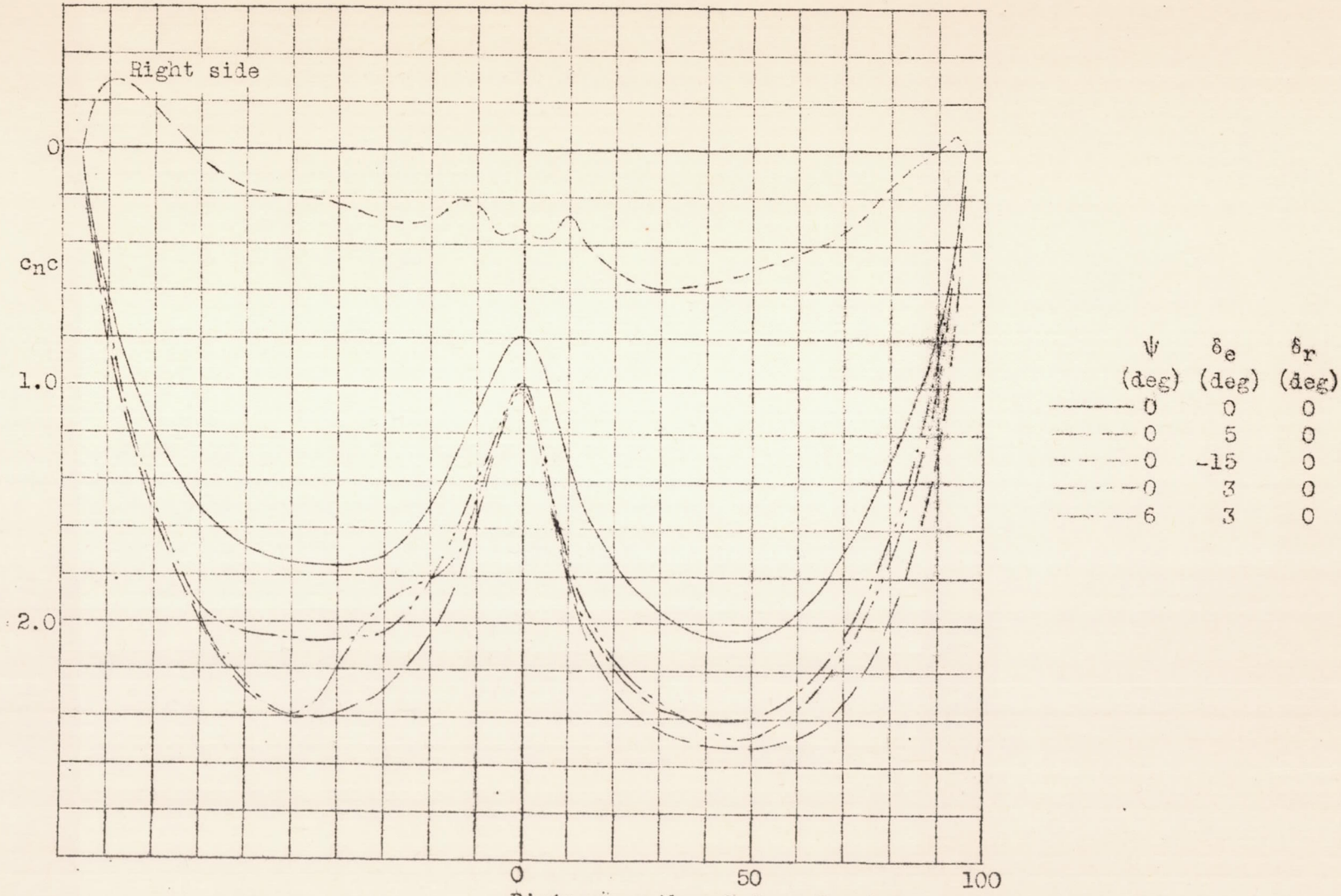

Figure 19.- Horizontal-tail span loadings, α_-,15.6°.

L-439

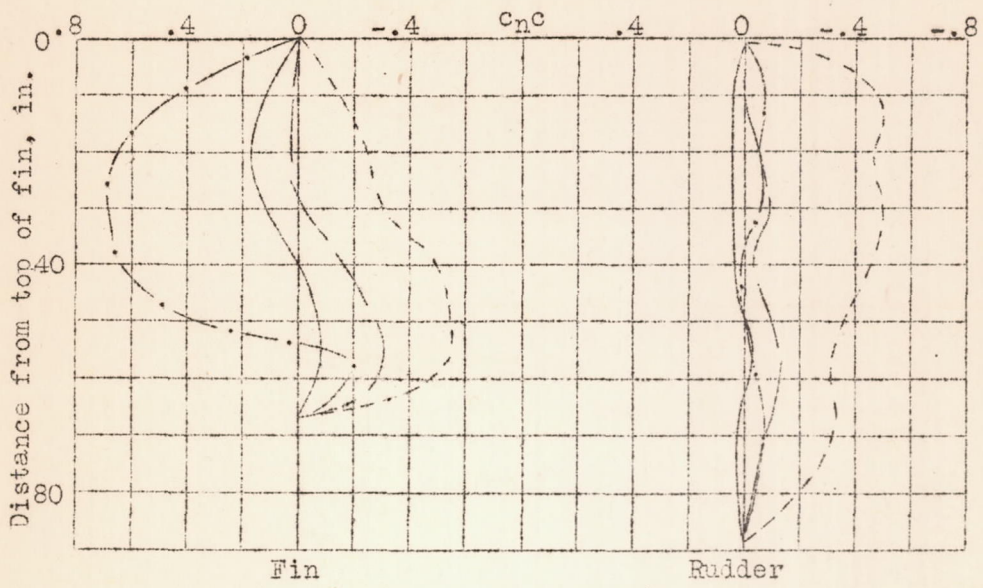

Figure 20.- Fin and rudder span loadings, α_T, 15.6°.

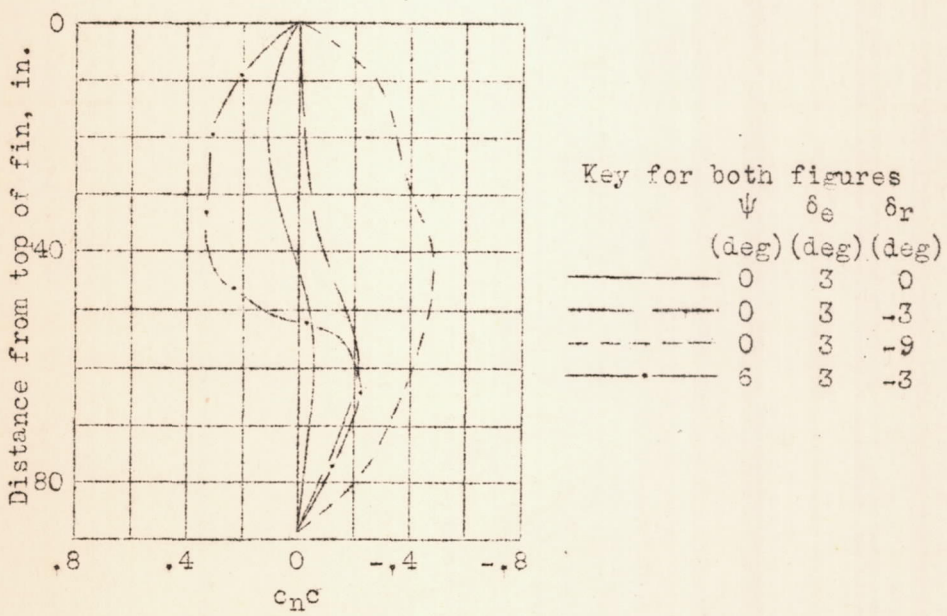

Figure 21.- Vertical-tail span loadings, α_T, 15.6°.

L-439

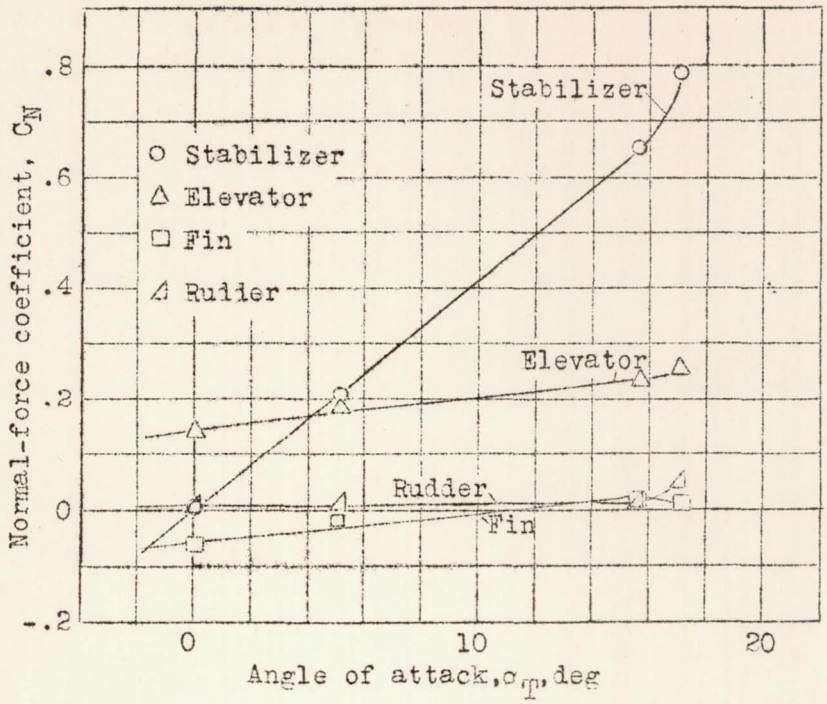

Figure 22.- Variation of normal-force coefficient with angle of attack, ψ, 0°; δ_e, 3°; δ_r, 0°.

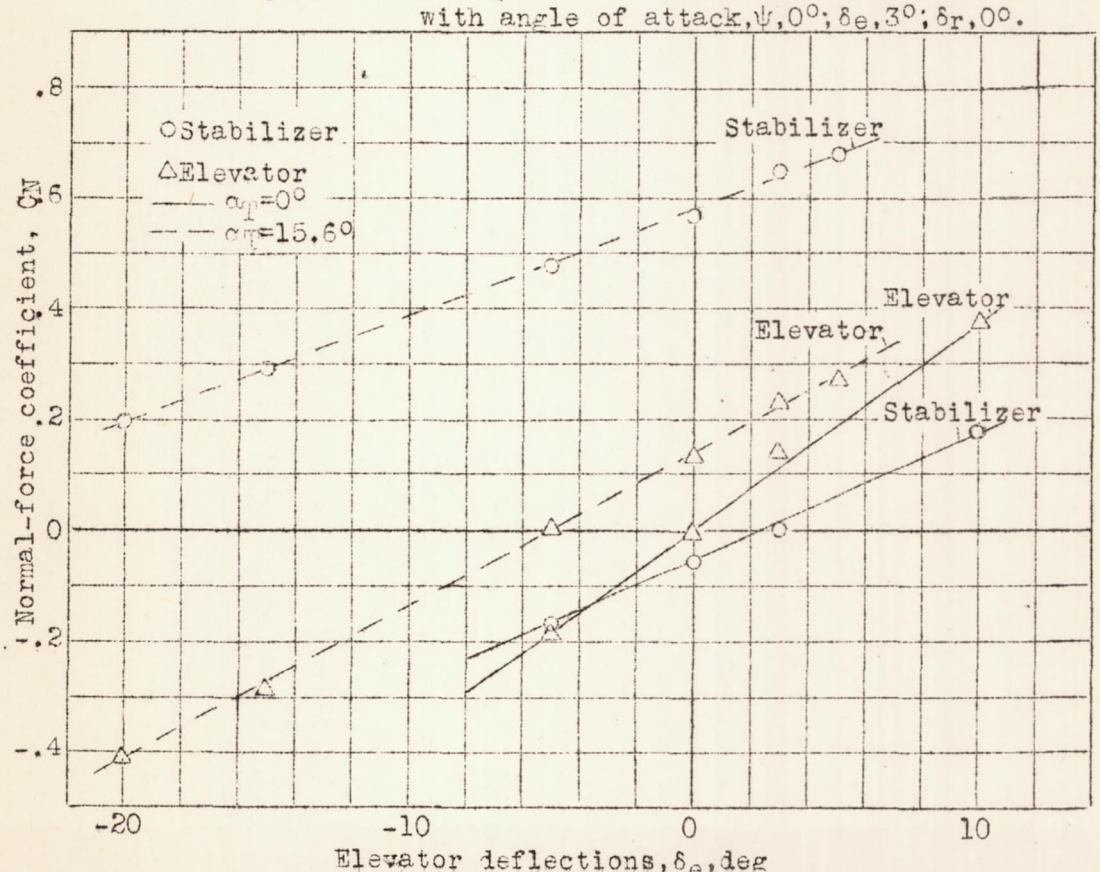

Figure 23.- Variation of the normal force on the stabilizer and elevator with elevator deflection for two angles of attack, ψ, 0°; δ_r, 0°.

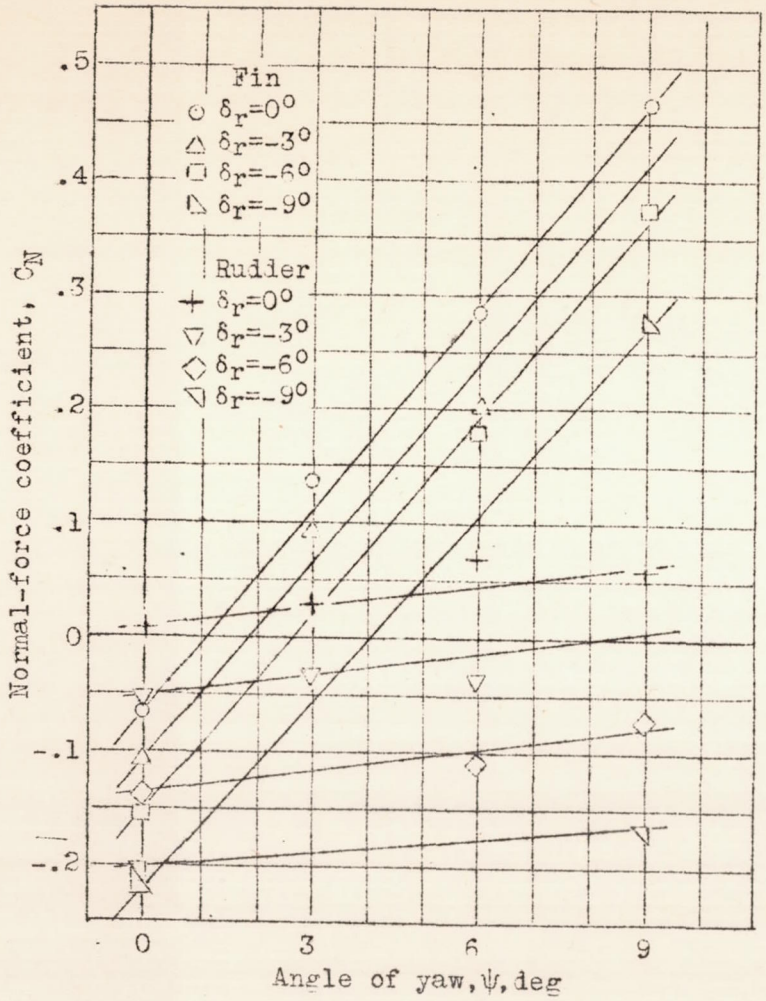

Figure 24.- Variation of normal-force coefficient for the vertical tail surface with yaw for several rudder deflections, α_T, 0°, δ_e, 3°.

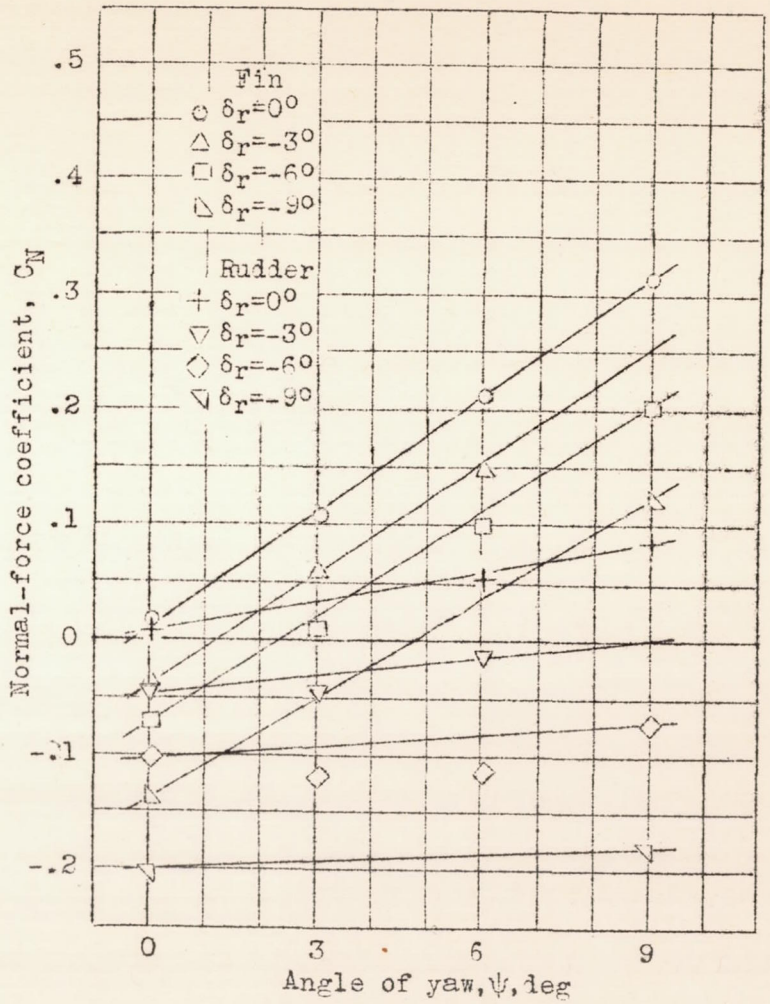

Figure 25.- Variation of normal-force coefficient for the vertical tail surface with yaw for several rudder deflections, α_T, 15.6°, δ_e, 3°.

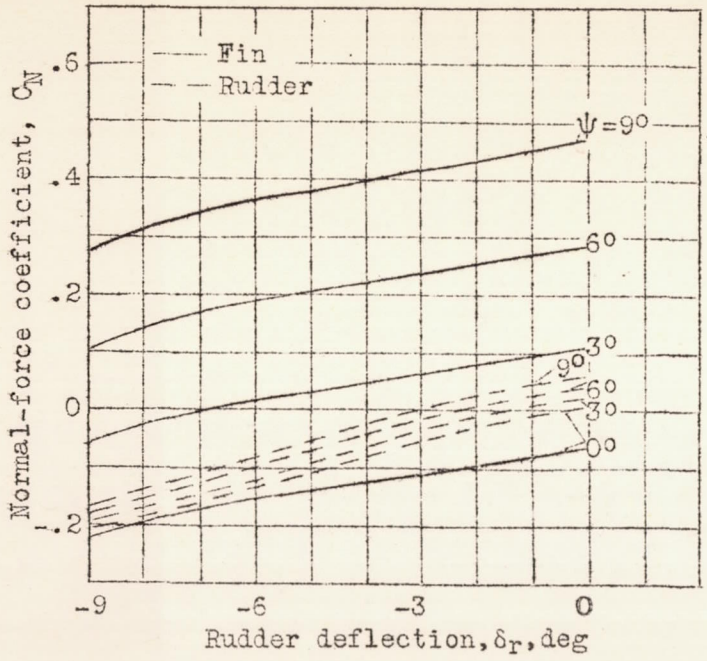

Figure 26.- Variation of normal-force coefficient for the vertical tail surface with rudder deflection and changing yaw, α_T, 0°; δ_e, 3°.

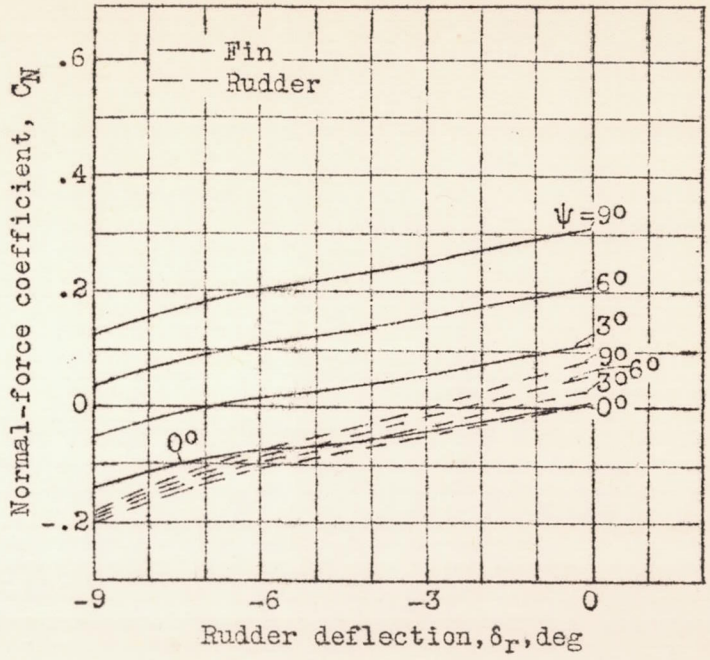

Figure 27.- Variation of normal-force coefficient for the vertical tail surface with rudder deflection and changing yaw, α_T, 15.6°; δ_e, 3°.

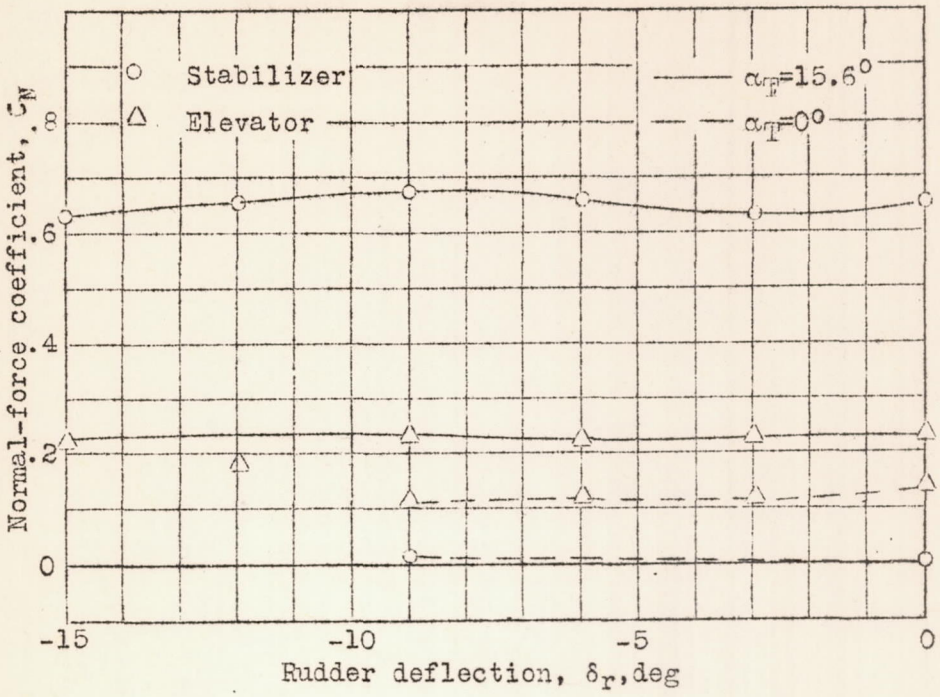

Figure 28.- Effect of rudder deflection on horizontal-tail loading, δ_e,3°.

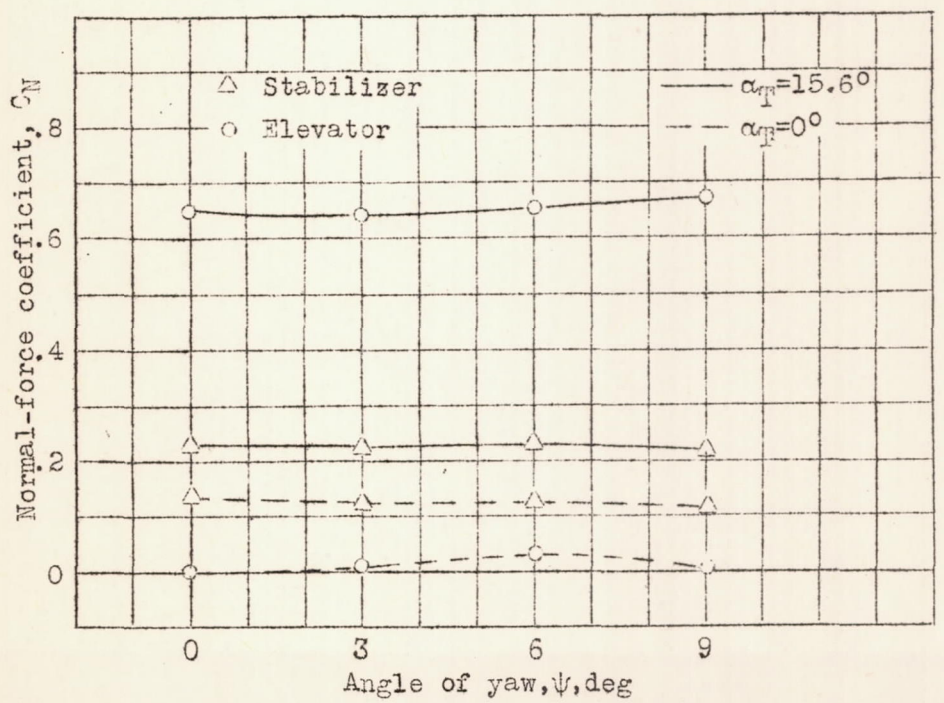

Figure 29.- Effect of yaw on horizontal-tail loading, δ_e,3°.

L-439

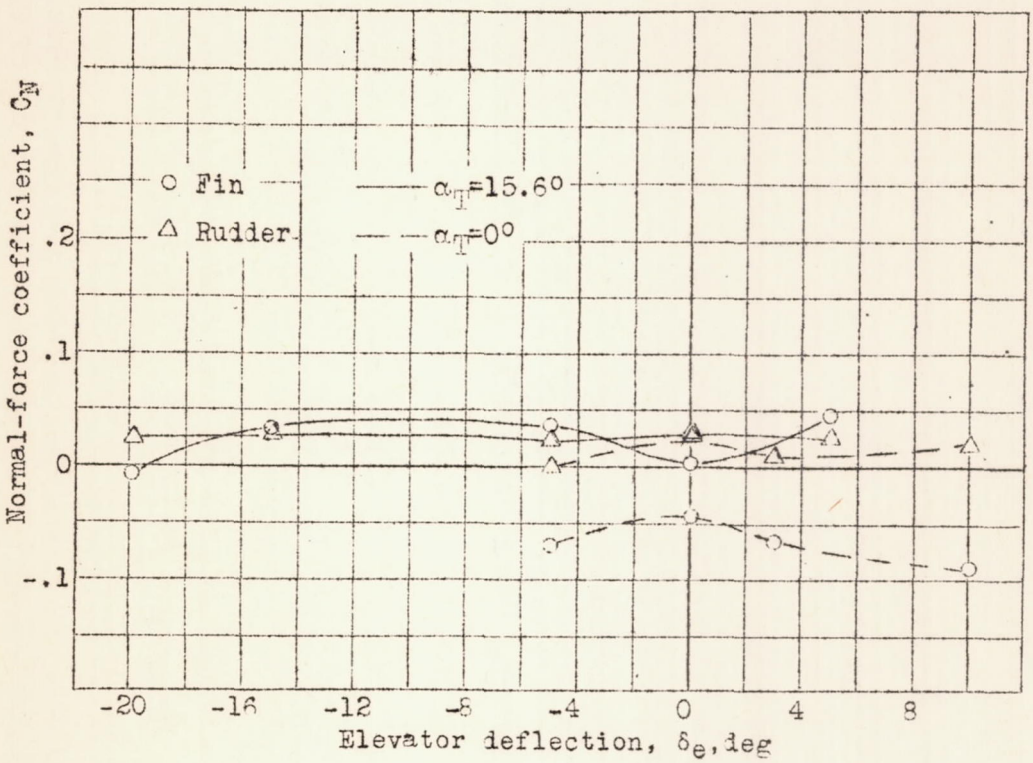

Figure 30.- Effect of elevator deflection on vertical-tail loading, δ_r, 0°.

A Distribution of dynamic-pressure ratio q/q_o due to wing wake
B Velocity distribution through fuselage boundary layer u/V_o
C Variation of q/q_o through fuselage boundary layer
D Combined effect of wing wake and fuselage wake q/q_o

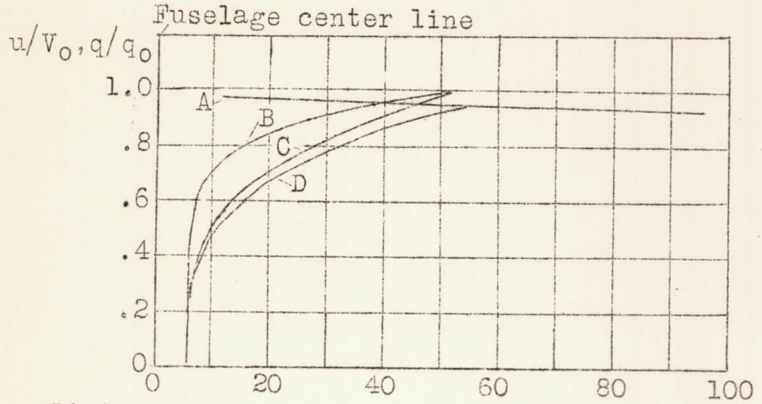

Figure 31.- Effect of wing and fuselage wakes on the dynamic pressure across the horizontal tail, α_T, 15.6°.

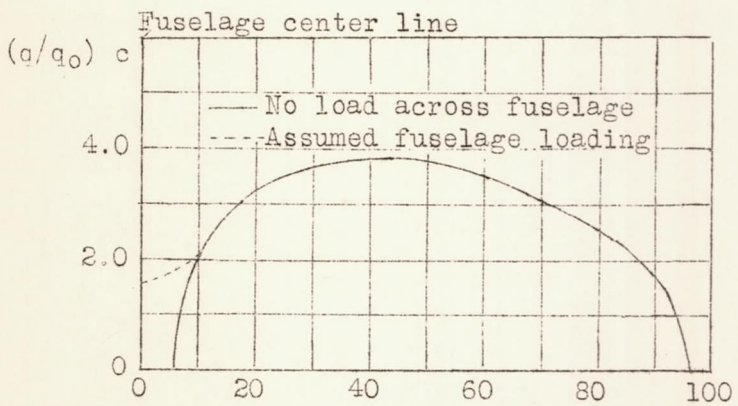

Figure 32.- Estimated span load distribution based on the dynamic-pressure ratio along the tail and the chord distribution, α_T, 15.6°.

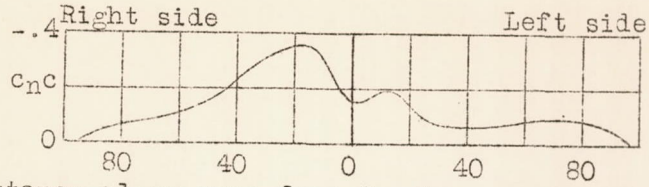

Distance along span from fuselage center line, in.

Figure 33.- Stabilizer span load distribution, α_T, 0°, δ_e, 0°.

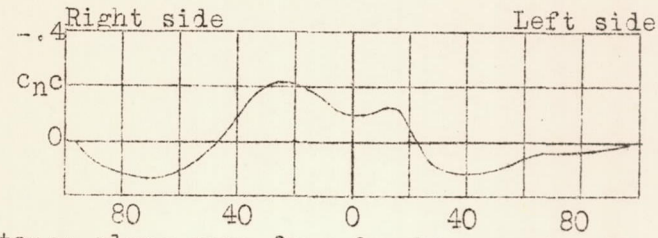

Distance along span from fuselage center line, in.

Figure 34.- Stabilizer span load distribution, α_T, 0°, δ_e, 3°.

Measured results from pressure distributions over the horizontal tail surface of the P-47B airplane.

—O— Based on free-stream dynamic pressure.

——— Based on local dynamic pressure.

Calculated results

— — — Isolated tail

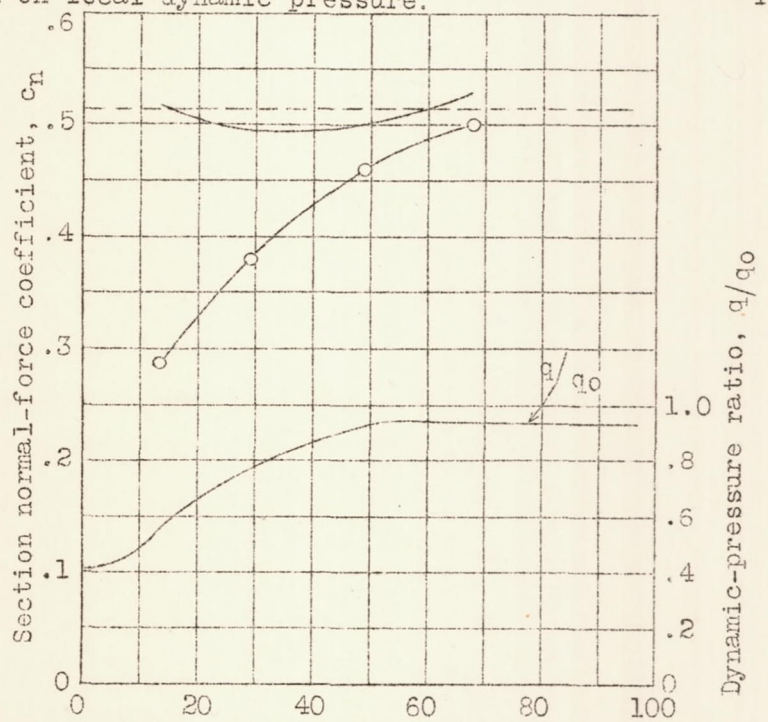

Distance along semispan from fuselage center line, in.

Figure 35.- Comparison of the measured and calculated normal-force distributions on the horizontal tail, α_T, 15.6°, δ_e, 0°.

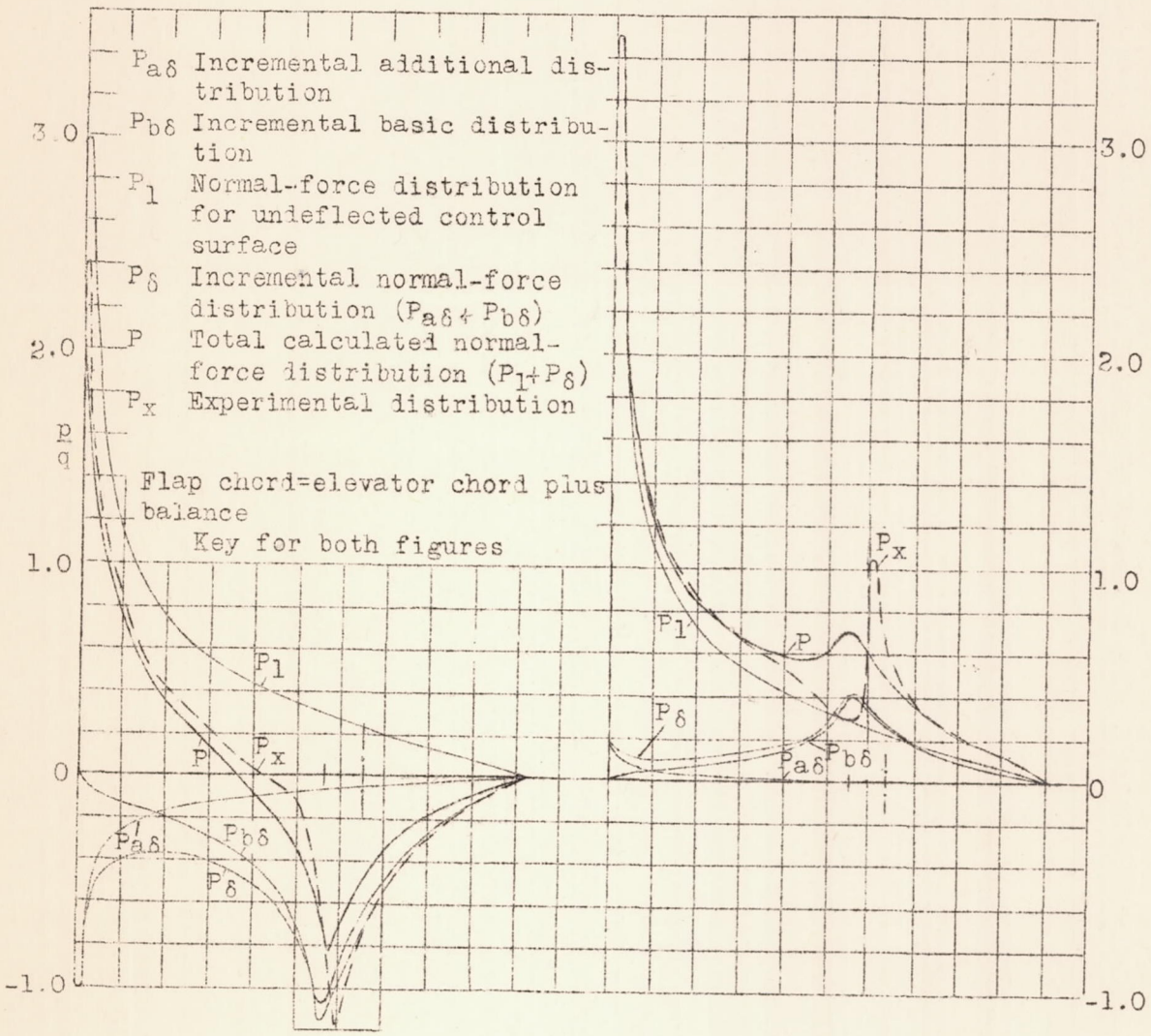

Figure 36.- Pressure distributions on rib 2.
α_T, 15.6°; δ_e, -15°.

Figure 37.- Pressure distributions on rib 2.
α_T, 15.6°; δ_e, 5°.

(Key for both figures given on figure 36)

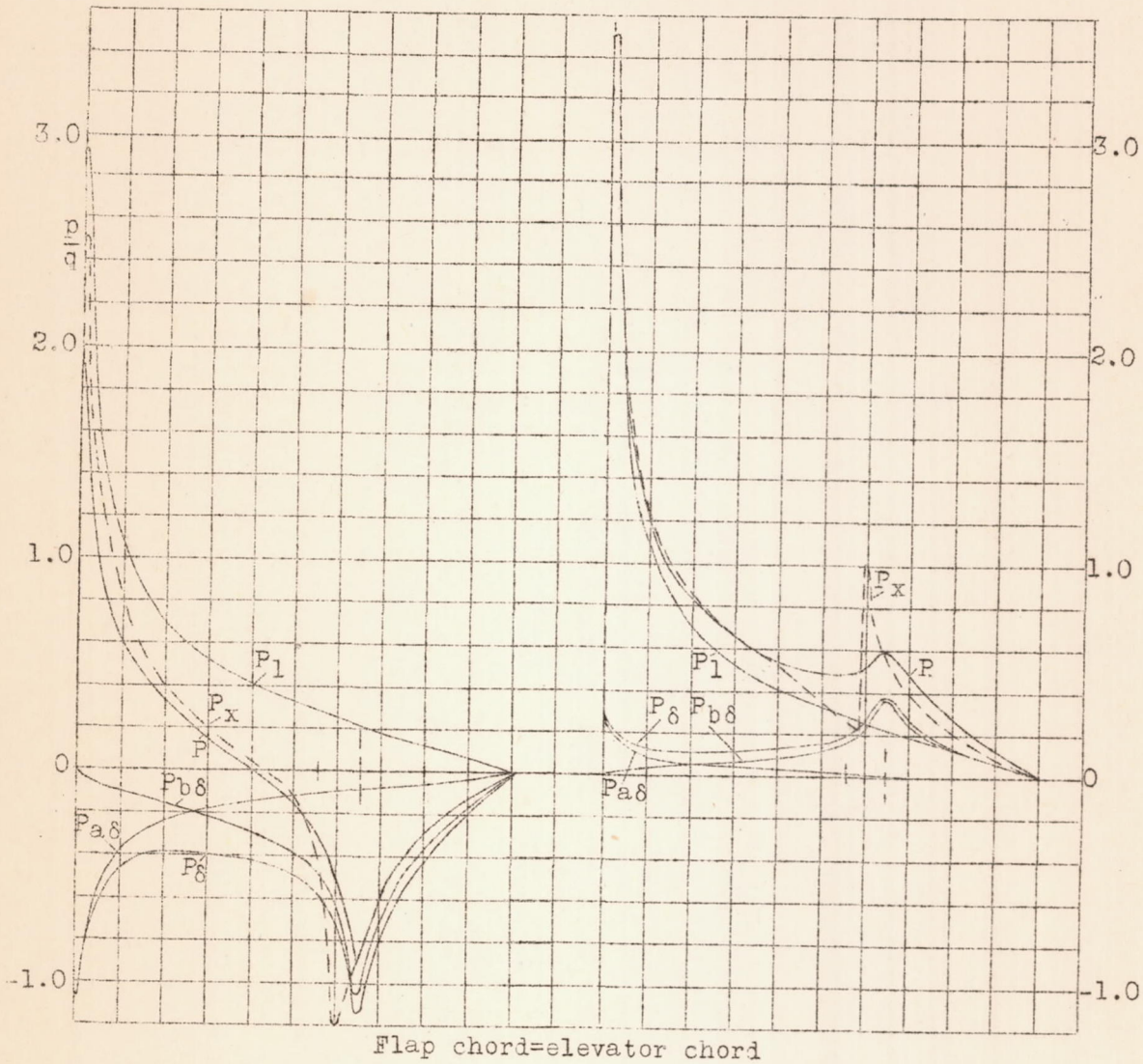

Figure 38.- Pressure distributions on rib 2.
α_m, 15.6°; δ_e, -15°.

Figure 39.- Pressure distributions on rib 2.
α_m, 15.6°; δ_e, 5°.